The effect of flexibly mounted piezoelectric eel on energy harvesting in the wake of a circular cylinder

Author

Muhammad Ramzan

Regn. Number

2019-NUST-MSME-00000318420

Supervisor

Dr. Izhar Ullah

DEPARTMENT OF MECHANICAL ENGINEERING

SCHOOL OF MECHANICAL & MANUFACTURING ENGINEERING

NATIONAL UNIVERSITY OF SCIENCES AND TECHNOLOGY

ISLAMABAD, PAKISTAN

November 22

The effect of flexibly mounted piezoelectric eel on energy harvesting in the wake of a circular cylinder

.

Author

Muhammad Ramzan

Registration Number

2019-NUST-MSME-00000318420

A thesis submitted in partial fulfillment of the requirements for the degree of

MS Mechanical Engineering

Thesis Supervisor:

Dr. Izhar Ullah

Thesis Supervisor's Signature: _____

DEPARTMENT OF MECHANICAL ENGINEERING

SCHOOL OF MECHANICAL & MANUFACTURING ENGINEERING

NATIONAL UNIVERSITY OF SCIENCES AND TECHNOLOGY

ISLAMABAD, PAKISTAN

November 22

FORM TH-4

Master Thesis Work

We hereby recommend that the dissertation be prepared under our supervision by **Muhammad Ramzan** (2019-NUST-MSME-00000318420), Titled: **The Effect of flexibly mounted piezoelectric eel on energy harvesting in the wake of a circular cylinder** be accepted in partial fulfillment of the requirements for the award of MS degree.

Examination Committee Members

Name: _____ Signature: _____

Name: _____ Signature: _____

Supervisor's name: _____ Signature: _____

Date: _____

Co-supervisor's name: _____ Signature: _____

Date: _____

COUNTERSINGED

Date: _____ _____

Dean/Principal

Thesis Acceptance Certificate

It is certified that final copy of MS thesis written by **Muhammad Ramzan** Regn. No. **2019-NUST-MSME-00000318420**, of SMME, has been vetted by undersigned, found complete in all respects as per NUST Statutes / Regulations, is free of plagiarism, errors, and mistakes and is accepted as partial fulfillment for the award of MS degree. It is further certified that necessary amendments as pointed out by GEC members of the scholar have also been incorporated in the said thesis.

Signature: _____

Name of Supervisor: **Dr. Izhar Ullah**

Date: _____

Signature (HOD): _____

Date: _____

Signature (Principal): _____

Date: _____

Declaration

I certify that this research work titled "**The Effect of flexibly mounted piezoelectric eel on energy harvesting in the wake of a circular cylinder***"* is my own work. The work has not been presented elsewhere for assessment. The material that has been used from other sources has been properly acknowledged/referred.

_____

Muhammad Ramzan

2019-NUST-MSME-00000318420

Certificate for Plagiarism

It is certified that MS Thesis Titled: by **Muhammad Ramzan** Regn. No.**2019-NUST-MSME-00000318420** has been examined by us. we undertake the follows:

a. Thesis has significant new work/knowledge as compared already published or are under consideration to be published elsewhere. No sentence, equation, diagram, table, paragraph, or section has been copied verbatim from previous work unless it is placed under quotation marks and duly referenced.
b. The work presented is original and the own work of the author (i.e., there is no plagiarism). No ideas, processes, results, or words of others have been presented as the Author's own work.
c. There is no fabrication of data or results which have been compiled/analyzed.
d. There is no falsification by manipulating research materials, equipment, or processes, or changing or omitting data or results such that the research is not accurately represented in the research record.
e. The thesis has been checked using TURNITIN (copy of originality report attached) and found within limits as per HEC plagiarism Policy and instructions issued from time to time.

Name & Signature of Supervisor

Name: Dr. Izhar Ullah

Signature**:** _____

Copyright Statement

Acknowledgments

I am thankful to my Creator Allah (SWT) to have guided me throughout this work at every step and for every new thought that you set up in my mind to improve it. Indeed, I could have done nothing without Your priceless help and guidance. Whosoever helped me throughout my thesis, whether my parents or any other individual was Your will, so no doubt none be worthy of praise but You.

I am profusely thankful to my beloved parents and siblings who raised me when I was not capable of walking and continued to support me throughout every department of my life.

I would also like to express special thanks to my supervisors Dr. Niaz Bahadur Khan and Dr. Izhar Ullah for their help throughout my thesis.

I would also like to thank Dr. Emad Uddin, Dr. Adnan Munir and Dr. Muhammad Sajid for being on my thesis guidance and evaluation committee and express my special gratitude to me for my help throughout the project.

I would also like to pay special thanks to Shaban Nawaz, Rizwan Mehmood and Muhammad Mahad for their tremendous support and cooperation. Without their help, I wouldn't have been able to complete my thesis. I appreciate their patience and guidance throughout the whole thesis.

Dedicated to my parent's soul, foster mother, loving siblings, and mentors whose untiring efforts and dedication boosted me to this wonderful achievement.

Abstract

The current method of producing energy from non-renewable sources may soon come to an end due to the ever-increasing demand for fossil fuels and the implications of escalating global warming. For microelectromechanical systems that only need a few watts of power to operate, an energy harvesting method based on wake flow energy is suggested. When a piezoelectric flag is employed as a cantilever beam and positioned in the wake of a bluff body, the strain exerted in the eel and the electrical voltage generated are ample to operate underwater sensors. The goal of this research is to present an efficient, simple, and resilient energy harvester that uses flow generated oscillations in response to ambient flow and fluid-structure interaction of flexibly mounted piezoelectric eel (pivoted mechanism) with inverted c-shape cylinder. Research objectives are to study the effect of spring stiffness and G_z (Gap along z-axis) on energy harvesting with varying Velocity. It was concluded from the research that by increasing the spring stiffness K_s i.e., 0.005-0.07 N/mm, velocity from 0.18m/s to 0.36m/s at G_z = 6 results in highest frequency of 0.0887Hz, amplitude to length ratio of 1.4361, and maximum amount of output power 9.25uW.Minimum values were obtained at bottom level of flow at G_z = 10, lower spring stiffness i.e., Ks=0.005 N/mm and lowest flow velocity of 0.18 m/s. While comparing the results with previous studies i.e., Circular, and inverted c-shape cylinder with mechanism of non-pivoted flag, significant amount of increment is observed in flapping frequency, amplitude to length ratio and output power which is **5.47%, 34.13%** and **61.12%** respectively.

Key Words:

Piezoelectric eel, bluff body, Energy harvesting, Inverted C-cylinders, Spring stiffness, Reynold's No.

Table of Contents

List of figures

List of Tables

Chapter 1: Introduction

The existing method of producing energy from non-renewable sources may soon come to an end, as demand for fossil fuels continues to rise and the consequences of rising global warming become more apparent. Their overuse has resulted in a plethora of problems, both environmental and economic[1]. As concern about serious environmental and ecological problems rises, the concept of creating green and renewable energy has grown in popularity and garnered significant attention in recent years[2]. As a result, scientists have concentrated their efforts on the brilliant concept of energy harvesting. It is a method of collecting energy that would otherwise be lost to the environment in the form of light, heat, sound, or vibrations. This research examines underutilized energy contained in vibrations emitted by a variety of sources, including bridge vibrations and marine risers. A piezoelectric energy harvester is a device that uses piezoelectric components to catch vibrations and convert them to electric power[3].

The Vibration Energy Harvester can be used to power wireless sensors in remote locations such as a bridge, a nuclear power plant, or oil and gas fields where crack detection is necessary, but battery charging is inconvenient[4]. If the energy from ambient vibration (i.e., bridge vibration) could be gathered, the battery could be recharged and would not need to be changed on a regular basis [5]. The classification of renewable energy harvesting sources are as follows in figure 1, amongst which a small-scale piezoelectric harvester is the

Figure 1.1: Renewable Energy Resources.

point of interest in this study.

1.1 Ambient Energy Scavenging

The need for a cordless electrical power source has generated interest in piezoelectric energy harvesting, or the extraction of electrical energy via a vibrating piezoelectric device[6]. To convert mechanical to electrical signals, a variety of effects can be utilized, including electromagnetic, electrostatics, electrodynamics, piezoelectric, and triboelectric. Due to its versatility and capacity to deliver high amplitude motion for high-frequency flapping, the PVDF flag is largely used as an energy collector[7]. When a piezoelectric crystal is positioned between two metal plates and is not under any stress, no electrical signal is produced since the charge is balanced. The piezoelectric crystal is subjected to mechanical stress caused by waves formed by a bluff body in a moving stream. In response to mechanical stress, positive and negative charges build up on the metal plates, generating enough energy to charge the sensors underwater[8].

1.2 Piezoelectricity

In a nutshell, a piezoelectric material generates an electric charge in response to deformation caused by external pressure or force. The piezoelectric material is electrically neutral in the absence of tension and deformation, implying that the positive and negative electrodes in the material coincide[9]. When mechanical pressure is applied to certain materials, the centers of positive and negative charges shift, resulting in the formation of an external electric field. During the inverse piezoelectric effect, an external electric field

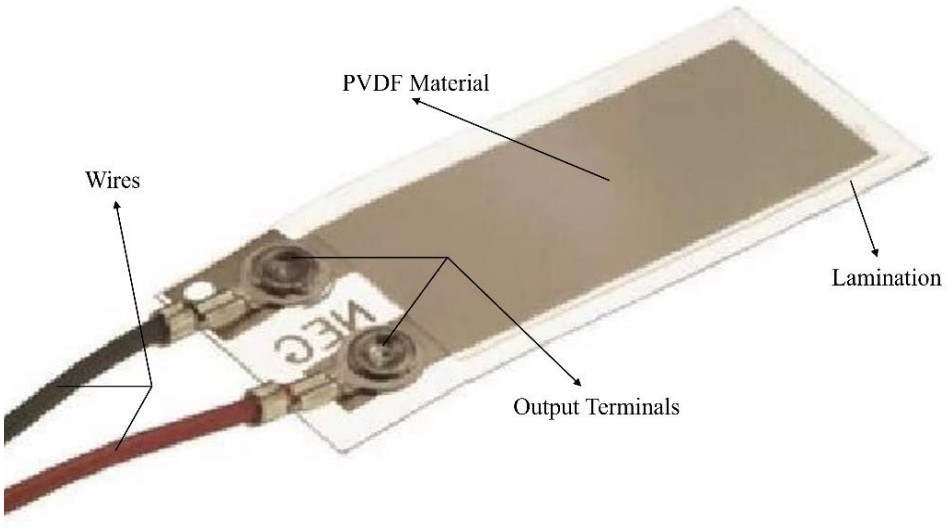

elongates or compresses the material, creating mechanical stress or pressure. There are both natural and man-made piezoelectric materials available [10].

Figure 1.2: The energy harvesting Piezoelectric eel

When the round cylinder is used as a bluff body, with the maximum pressure at the stagnation point, the wake is formed[11]. The pressure steadily decreases in the first half of the cylinder before rising in the second half. The flow particles are exposed to an unfavorable pressure gradient, causing the flow to detach from the bluff body's surface and create the wake, which is a highly turbulent zone. When a divided boundary layer produces a shear layer, it rolls into a certain shape and detaches from the surface, causing vortex shedding. The rolling pattern is determined by the size and shape of the bluff body, as well as the Reynolds number of the flow. When these shear layers alternately shed and produce a vortex pattern in the wake region, the Karman vortex street is generated. Vortex-induced vibration is created by the pressure distribution that occurs when the vortices are shed[12-14].

1.3 Benefits of the PVDF flag

The following criteria affected the choice to utilize a piezoelectric flag for energy harvesting:

- It can adapt to impinging vortices created by the bluff body using the Karman Vortex Street pattern as a guide[10].
- It moves with a strong amplitude and a high flapping frequency, similar to how a flapping flag moves[15].

1.4 Background of Study

Most of the research in recent years has focused on the flapping dynamics of piezoelectric membranes in a fluid flow. As the vortices collide with the piezoelectric membrane, it vibrates. Two procedures are used to convert energy. The kinetic energy of the water is turned to mechanical strain energy in the piezoelectric flag, which is subsequently converted to electrical energy[16].

Previous experimental and numerical studies have established that the accumulated power is exactly proportional to the frequency and area of the flapping[17]. Maximizing this power is an excellent topic. In the case of a bluff body, pressure drag dominates, whereas viscous drag dominates in the case of streamlines. The flow is governed by drag, which is entirely dependent on the shape of the body included inside the flowing path of a fluid[12]. At a small attack angle, the airfoil behaves like a streamlined body; at a large attack angle, it behaves like a bluff body[18]. When brick or any other shape of the cylinder causes pressure drag, a separation region forms; therefore, there are different types of bluff bodies. The size of the wake is mostly determined by this separation zone, and the pressure is reduced because of eddy formation. This decrease in pressure results in pressure drag. When a more acute angle of attack airfoil is used as a bluff body, the flow over its top surface is split, resulting in a pressure drag that is significantly larger than the viscous drag[13]. It is a creeping flow at low Reynolds numbers. With increasing Reynolds number, the vortex street transforms from laminar to turbulent, and then from laminar separation layer to turbulent (lower transition regime). Trans-critical flows cause the boundary layer to become totally turbulent on both sides[19].

1.5 Research aims and objectives

The goal of this research is to present an efficient, simple, and resilient energy harvester that uses flow generated oscillations in response to ambient flow and fluid-structure interaction of flexibly mounted piezoelectric eel with inverted c-shape cylinder.

Research objectives are:

- To study the effect of spring stiffness (Ks) on energy harvesting with varying velocity
- To study the effect of varying Reynold's number on energy harvesting
- To study the effect of changing Gap along z-axis (Gz) i.e., across length of cylinder on energy harvesting

1.6 Thesis structure

This research study's background and literature review will be detailed in Chapter 2. The experimental strategy and methods for determining harvested power, flapping frequency, and oscillation amplitude are presented in Chapter 3. The experimental data is collected and evaluated in Chapter 4, also the results are reviewed in Chapter 4, and the conclusions are discovered in Chapter 5.

Chapter 2: Literature Review

Usman Latif *et al.* experimentally studied the piezoelectric energy harvesting in the wake of a circular cylinder using a wind tunnel by tuning the S/D, L/D, and flow velocity parameters. The frequency and output voltages were measured by using a camera and oscilloscope respectively. The study aimed to explore the range of piezoelectric eel in vortex shedding wake to harvest maximum energy. Almost 38% increment in voltage was observed when flow velocity was increased from rest to 10m/s, and maximum energy was extracted from piezoelectric eel by adjusting the parameters L/D (ratio of the membrane length to the cylinder diameter) to 1 and S/D (ratio of the distance between the cylinder and membrane to the cylinder diameter) to 2[12].

Gao, Zong et al. numerically investigated the effect of the aging of a circular cylinder on energy harvesting and vortex-induced vibration. The circular cylinders of different roughness are used as a bluff body and PVDF piezoelectric eel is used as an energy harvester. The oscillating amplitude, flapping frequency, and RMS voltage obtained on the terminals of eel are compared and concluded that within the increase of roughness, the drop in amplitude and frequency is noticed. Due to the low speed of flapping of the leading edge of the eel and less amplitude covered, small numbers of charges were collected which means that the drop in power will be occurred when a bluff body is overaged. The roughness parameter is found as Ks/D to non-dimensionalize the research study. More drop in amplitude is found than that of frequency w.r.t the roughness. The value of Ks/D is recommended after which the cylinder must be replaced[20].

Wang, Zhang *et al.* studied the experimental effect of the rectangular plate in the wake of the circular cylinder results in increased energy harvesting using flow-induced vibration in the wind spectrum. The basic purpose of this study was to locate the position of the rectangular plate, its effective design dimensions to gain maximum power. Several wind tunnel experiments were carried out to justify the effectiveness of the plate in wake of the circular bluff body, which results in a positive change of output when we increase the distance between cylinder and plate. Galloping response was obtained when space between plate and cylinder was decreased, and lock-in response was obtained when the distance between plate and cylinder increased, and height of plate decreased. The optimal design parameters exhibit the 2D height of the plate and $0.2D \approx 0.4D$ space between cylinder and plate (where D is the width of the rectangular plate) to obtain effective performances within the lock-in region and increased wind speed for energy harvesting[21].

Ding, Zhang et al. investigated numerically Flow induced motion and energy harvesting from cylinders having different cross-sections using 2D unsteady RANS model in the Reynold number range from 10,000 to 130,000 and verified with experimental results also. Different cross-sections of cylinders used in the study were PTC-cylinder, quasi trapezoid, square and triangular prism. The behavior of amplitude and frequency response can be observed in four different branches i.e., VIV initial branch, VIV upper branch, the transition from VIV to galloping, and galloping. PTC-cylinder and Q trapezoid 1 have better performances in FIM response and energy harvesting (maximum energy efficiencies of said cylinders are 45.7% and 37.9% respectively) as compared to other cylinders. The maximum amplitude of 3.5D was achieved in the galloping region and optimum energy was harvested in VIV upper branch at Reynold number greater than 30,000[22].

Tamimi, Naeeni *et al.* experimentally studied the vortex shedding effect of flow-induced vibration of the right-angled triangular cylinder and compared the results with circular, square, and diamond-shaped cylinders. They examined different configurations of a triangular cylinder having a flat face and vertex edge concerning flowing fluid. They concluded that a galloping type of response can be observed when the flat face of any sharp edge cylinder is kept perpendicular to the incident flow, it is the case of the square cylinder and two flat face configurations of the triangular cylinder. On the other hand, VIV type response can be observed when the sharp edge of the diamond and triangular cylinder is kept perpendicular to flowing fluid. The isosceles triangular cylinder has 6 times more galloping response as compared to the square cylinder causing high phase lift force and ultimately increased oscillation amplitude and relatively high hydro elastic efficiency[23].

The purpose was to study the vibration characteristics of long flexible cylinders subjected to vortex-induced oscillation. Emphasis was placed on the investigation of the relationship between in-line and crossflow vibration. Under non-lock-in, random vibration conditions, the linear spectral analysis indicated that in-line and crossflow responses were linearly independent of each other, while the results of the modal analysis showed that the moving average vibration energies in these two directions were strongly related. A higher-order spectral analysis was performed to demonstrate a non-linear correlation between in-line and crossflow vibration of flexible cylinders excited by vortex shedding in both uniform flows and sheared flow conditions. The results of the bispectral analysis demonstrated the existence of a quadratic relationship between in-line and crossflow motion under both lock-in and non-lock-in conditions. The well-known frequency doubling phenomena in in-line response was proven to be the result of such a quadratic correlation[24].

Vai Kuong Sin was able to do a numerical analysis to determine how a piezoelectric eel interacts with a vortex that is shedding behind a bluff body. The impacts of other variables, including flow speed, eel length, and the breadth of the bluff body, were also intended to be explored. The results together with the Arbitrary Lagrangian-Eulerian (ALE) approach effectively approximated the undulating motion of the eel[25]. Nor Fakhzan Mohd In order to identify the ideal bluff body for a piezoelectric eel, Mohd Kazim performed a 2-dimensional computational fluid dynamics (CFD) simulation study of the wake region produced by inserting several bluff bodies, including U-shape, D-shape, triangle, square, and cylinder. The findings showed that, within a particular range, a triangle-shaped bluff body is the most effective form for inducing vortex shedding in piezoelectric eels[26].

Vortex-induced vibrations boost tunnel energy collecting. Inverted C-shaped cylinders with various cut angles are positioned in uniform fluid flow to collect electrical energy from piezo-flag in downstream vortices. Experiments indicate insufficient and optimal wake coupling. Streamwise gap and flow speed impact piezo-flag amplitude and flapping frequency. Inverted C-shaped cylinders with 120-degree cut angles provide 66% more power than round cylinders. Vortex shedding yields no energy utilizing piezo flag for each cylinder and flow velocity due to poor wake flow coupling. Data show circular and inverted C-shaped cylinders collect energy equally. Form and cut angle affect flapping amplitude, growth rate, and dominant frequency. Wake dynamics mirror the energy efficiency gain in PIV trials. 120-degree cut angle is better than round cylinder as fluid energy harvester kinetic source. Tuning the inverted C-streamwise cylinder's spacing, flow velocity, and cut angle harvests vortex energy[27].

VIVACE is a revolutionary technique that gathers hydrokinetic energy from ocean currents by boosting Vortex Induced Vibration (VIV). In this article, the VIV of an elastically attached circular cylinder in a towing tank water channel is experimentally tested to explore the influence of natural frequency utilizing five different springs (125 N/mK495 N/m). The cylinder oscillates transversely in a subcritical Reynolds domain (1.5104Re6104) with a strong mass-damping parameter (m* = 0.11). VIV strongly depends on natural frequency and lock in in a wide range of spring stiffness. The analyzed Re range demonstrated the progressive shift between two turbulent shear layers from Re4,000 to Re100,000. Spring stiffness boosts the top branch's synchronization ratio and range. In experiments, strong mass-damping eliminated the lower response branch. These data propose using an adjustable natural frequency approach for optimal energy harvesting in VIV-based ocean energy converters[28].

Vortex-induced vibration (VIV) is the turbulent motion created on bluff body that produces alternate lift forces and leads to erratically moving the body. The VIV-powered system appears like a fantastic idea for greening the energy industry, and its ability to use the water's slow current speed to produce electricity is maybe its most crucial feature. The purpose of this article is to examine the impact of spring stiffness on the VIV characteristic. It's crucial to do the study to transform these potentially harmful vibrations into a useful source of energy. To investigate the behavior of VIV, five cylinders measuring 0.25 to 2.00 inches in diameter are examined. The results of this experiment show that the 2.0-inch cylinder had the lowest inaccuracy in frequency ratio, 1.1%, and a high likelihood of lock-in state. In terms of maximum amplitude, this cylinder produced oscillation motion with the largest amplitude, which is equal to 0.0065 m[29].

Chapter 3: Methodology

A water tunnel is available in the Department of Mechanical Engineering, SMME, NUST Pakistan, where the experimental work is carried out. Water tunnel, centrifugal pump, honeycomb structure, variable frequency driver for the motor, camera, piezoelectric flag, bluff body, source light, DAQ card, laser, and laser modulator are all components of the experimental setup. A low speed closed flow configuration is used in the water tunnel. A centrifugal pump that has a speed range of 0 to 0.5 m/s and is driven at a frequency that can be adjusted from 0 to 50 Hz is used to circulate water through a tunnel[30].

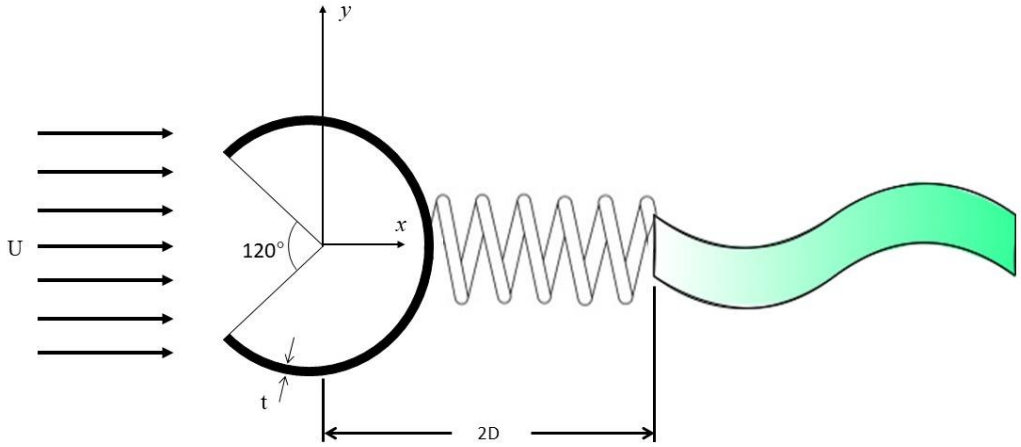

Figure 3.1: Schematic of setup having flexible leading end of flag and free trailing end (top view)

3.1 Experimental Parameters

Three experimental parameters were studied during the research which include

- The behavior of Springs having different stiffness $\mathbf{K_s}$ (0.005-0.07 N/mm) attached with leading edge of flag on flapping frequency, peak-to-peak amplitude, and energy harvesting.
- Second parameter was to change the vertical gap of flexibly mounted eel from free stream surface of water along the Z-axis i.e., across the length of cylinder, and this vertical gap is non- dimensionalize by dividing with cylinder diameter and referred as $\mathbf{G_z = L/D}$.
- Third parameter was to vary the fluid velocity from 0.18-0.36 m/s, against which Reynold's number is also calculated given in Table 3.

Above mentioned parameters with their values are given below in table

Table 1: Experimental Parameters

Parameters	Value
K_S (N/mm)	**0.005, 0.023,0.027, 0.05, 0.07**
Gz = L/D	**2, 4, 6, 8, 10**
Velocity (m/s)	**0.18, 0.24, 0.30, 0.36**

3.2 Spring Stiffness (K_S)

Frequently, F = -kx is used to represent the spring constant, where F stands for force and x for displacement. Simply said, the negative symbol denotes that when a spring's end is moved to the right, it pulls left, and vice versa[31].Springs were locally manufactured with stainless steel wires and length of spring was fixed as 2D (doubled the diameter of cylinder i.e., 50mm from the center of cylinder). After manufacturing, stiffness of springs was measured using Universal Testing Machine (100 kN) at Mechanics of Material lab, SMME NUST. The value of k gives the stiffness of the spring, in N/mm as shown in table 2.

Table 2: Spring Stiffness measurements

Sr. No.	Max. Force F (N)	Max. Disp. x (mm)	Spring Stiffness $K = \frac{F}{x}$ (N/mm)
1	1.4	20	0.07
2	1	20	0.05
3	0.8	30	0.027
4	1.53	65.21	0.023
5	0.49	100	0.005

3.3 Reynold's Number

It measures the relationship between inertial and viscous forces. If the flow is turbulent or laminar, it may be determined by the Reynolds number. A laminar flow occurs when a fluid's viscosity dominates the effects of inertia. Turbulent flow is a term used to describe a flow in which the inertia force dominates the viscosity. Laminar flows have a Reynolds Number of less than 2300, whereas turbulent flows have a Reynolds Number of more than 4000.

The formula gives Re its mathematical definition[32].

$$R_e = \frac{\rho UD}{\mu}$$

Table 3: Reynold's number Calculations

	Fluid velocity	**Reynold's No.**
Fluid density ρ = 998 Kg/m3 Fluid viscosity μ = 1.0016 Ns/m2 Diameter of the fluid D = 25mm	U (m/s)	$R_e = \frac{\rho UD}{\mu}$
	0.18	4484
	0.24	5978
	0.30	7473
	0.36	8968

3.4 Blockage Ratio

In an experimental study conducted in 1998, Choi looked at the square model wind tunnel's blockage ratio. The ratio of the tunnel's width to the diameter of the cylinder in use is known as the blockage ratio. The boundary layer's thickness grows as the blockage ratio rises. According to his studies, a 10% blockage ratio may be tolerated with just little consequences on the trials {Choi, 1998 #58}.

3.5 Energy Harvesting Eel

A cutting-edge invention called the Energy Harvesting Eel uses piezoelectric polymers to transform mechanical flow energy from the oceans and other rivers into electrical power. These systems are expected to play a significant role in autonomous marine sampling networks in the future. This energy-harvesting gadget makes use of long strips of piezoelectric polymers that move up and down in a water flow in a manner akin to an eel swimming. Future Eels may employ a more effective electro strictive polymer like PVDF {Allen, 2001 #59}.

In the investigation we conducted, a piezoelectric flag (DT2-028 K/L) was employed. The mechanical, electrical, and material parameters of the piezoelectric flag are shown in the accompanying tables {Specialties, 2006 #60}.

Table 4: Piezoelectric eel Specifications

Eel/Flag	**Material**	**PVDF**
	Size	72 mm x 12 mm x 64 µm
	Density	1.78 kg/m3
	Poisson ratio	0.46
	Young's modulus	1.38 GPa
	Capacitance	1.44 nF
	Membrane thickness	28 µm
	Storage temperature	-40 °C to +70 °C
	Operating temperature	0 °C to +70 °C
	Voltage range	10 mV – 100 V

3.6 Experimental Setup

The closed loop water tunnel used for all of the tests included a transparent test section that was 2000mm long, 400mm wide, and 500mm high. A flat-type wave maker that was mounted to one end of the tunnel was used to produce waves for the trials. A vertical mesh style wave absorber was utilised on the other side of the tunnel to block incoming waves and lessen wave reflections.

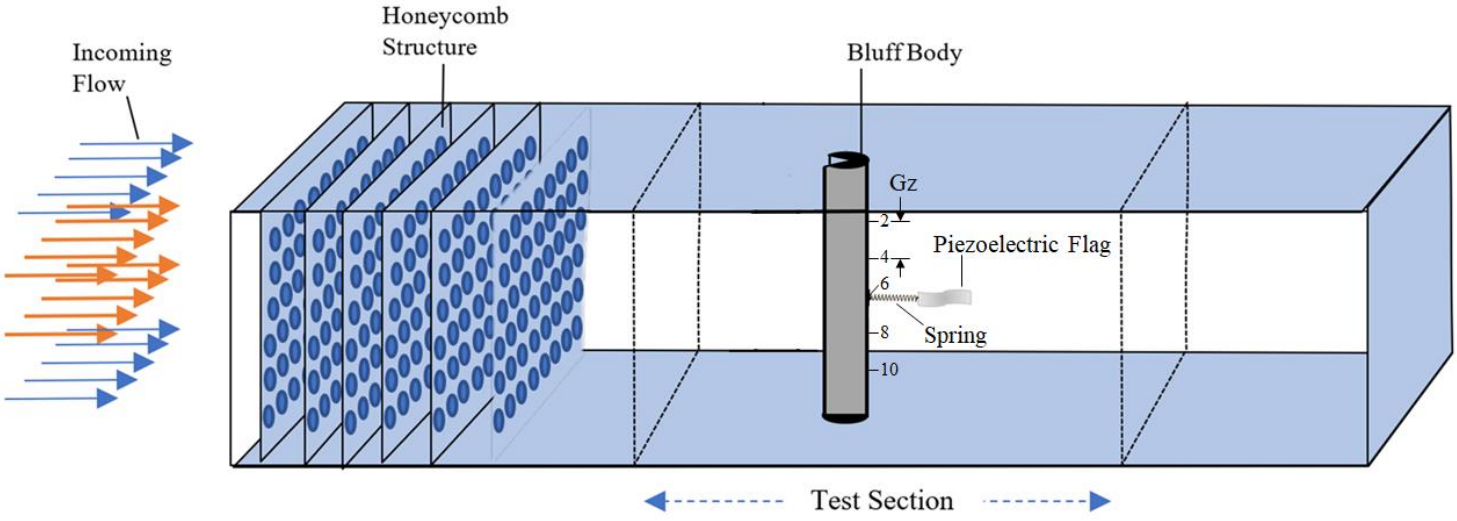

Figure 3.2: Schematic of complete experimental setup

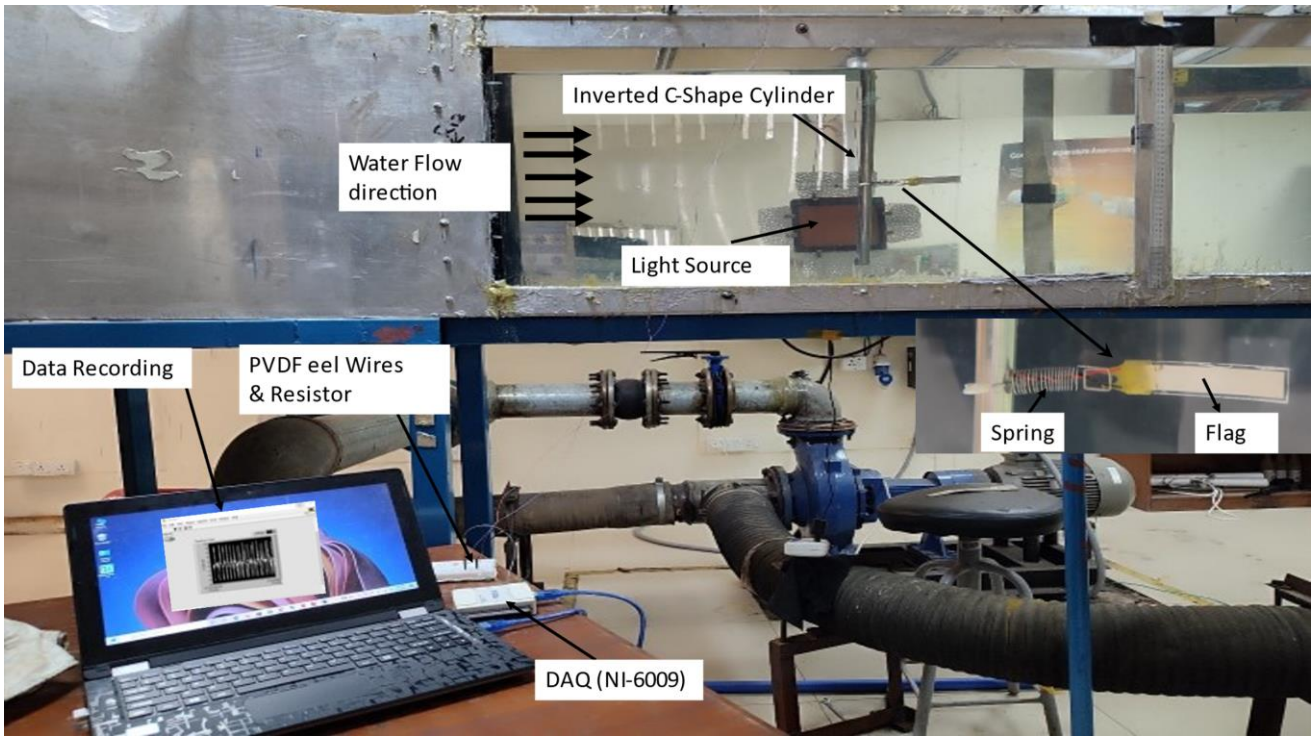

Figure 3.3: complete physical setup with flexibly mounted piezoelectric eel in wake of an inverted C-shape cylinder

In the water tunnel before to the test portion, there are a few aluminium honeycombs placed with dimensions of 1.83 metres in length, 0.55 metres in width, and 0.025 metres in height. This hexagonal opening honeycomb's function is to provide a streamlined flow for testing. The entire Experimental setup is depicted schematically in the pictures{Saeed, 2018 #55}.

Table 5: Parameters and values used in Experimentation

Parameter	Unit	Value
Cylinder diameter (D)	mm	25
Thickness(t)	mm	1.5
C-section cut angle(α)	Degree (°)	120
Blockage ratio	%	6.25
Velocity (U)	m/s	0.18-0.36
Gz= L/D		2-10
K_S	N/mm	0.005-0.07
Optimal resistance	MΩ	1

The mounting mechanism of setup in which flexibly mounted piezoelectric eel is attached with bluff body parallel to flow direction is shown in figure 3.4. Data is recorded for different spring stiffnesses along with mount position of spring across vertical length of cylinder and all cases are recorded with varying the velocity of fluid. And total cases in study were **5*5*4 = 100**

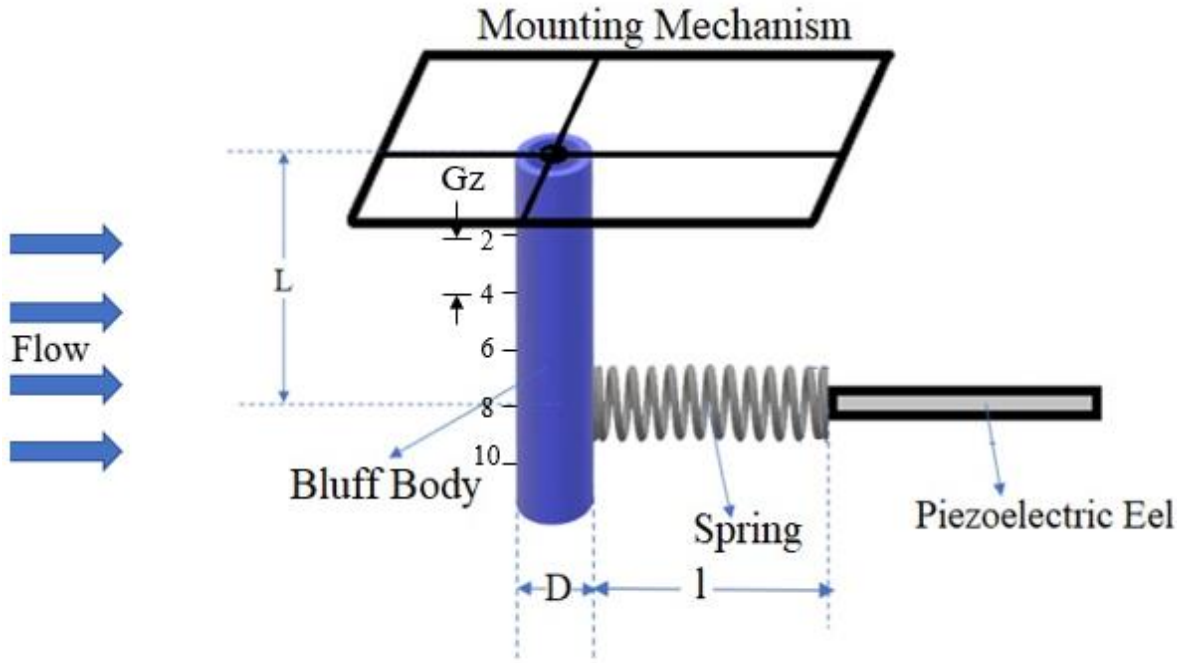

Figure 3.4: Schematic of Experimental Mechanism (Side view)

Where,

D: diameter of cylinder in mm (bluff body)

l: length of spring (mm)

K: Stiffness of spring (N/mm)

L: Length from free surface of water to spring connection point

3.7 Data Collection

The voltage produced by the piezoelectric flags was calculated using a data collecting system called DAQ (a module in National Instrument Lab View). A sampling rate of 50 samples per second was used to monitor voltages, which implies that 50 voltage samples are taken in a second. The indicator reads the data from Lab View and presents it as a number, or in the form of charts or bars, for further processing, once the assistant has acquired the data from the DAQ {Saeed, 2018 #55}.

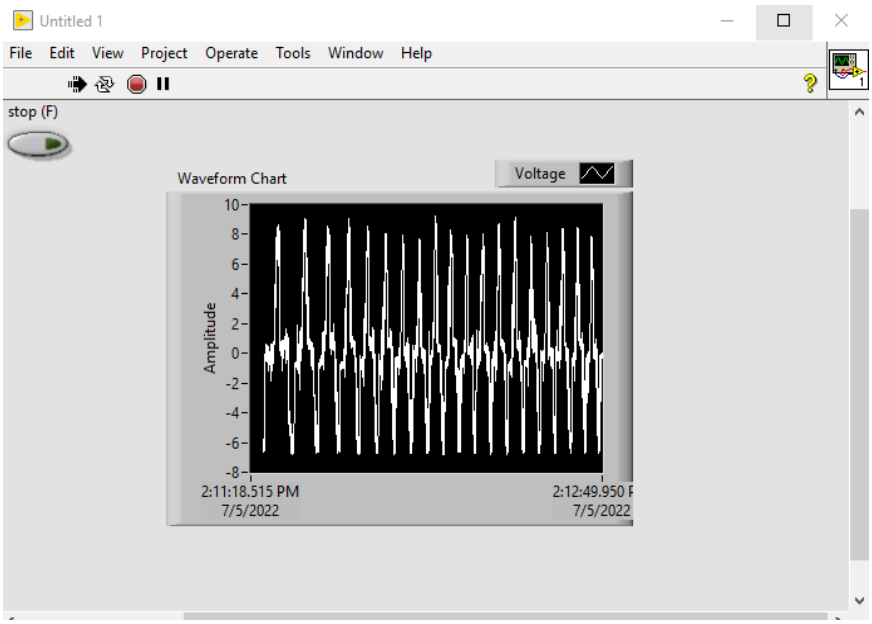

Figure 3.5: Voltage signal using DAQ (NI USB-6009) in LabView software

The movement of the piezoelectric flags was captured at a rate of 50 frames per second using a high-speed camera (a Sony RX100 IV) that was positioned below the bottom of the test section to gather photos of the piezoelectric flags when they were in a flapping condition. For the vision of the flags in the flow, two torches were utilized from both sides of the test portion of the water tunnel. Additionally, the upper side of the test section was covered with a black fabric to make the flag visible. Images were examined in MATLAB by employing an image processing approach to detect the tail position of the flags to compute the peak-to-peak amplitude (A/L) and overlaid images of the flags (Flapping envelope) for the greatest and minimum flapping amplitude.

This data is used to determine the root mean square value (Vrms). The gathered power is determined using this formula in accordance with Ohm's law.

$$P = \frac{{V_{rms}}^2}{R}$$

Where P is the power that has been harvested, Vrms is the RMS value of voltage data that has been collected for approximately 120 seconds, and R is the ideal resistance, which is 1 M in accordance with the maximum power transfer theorem {Kong, 1995 #61}.

Chapter 4: Results & Discussion

A piezoelectric flag experiences strain when it is put in the fluid trail left behind by the insertion of a bluff body. The produced strain in the eel is a function of time as well because of variations in a wave's wavelength, vortex type, amplitude, and frequency. Piezoelectric action causes this pressure/strain energy to be transformed into electrical voltage. The strain rate, coupling coefficient, flapping frequency, amplitude, and piezoelectric eel's specifications all affect the amount of power that can be gathered. The flapping frequency cube and oscillation amplitude directly affect how much electricity is collected {Shoele, 2016 #62} {Mitcheson, 2008 #63}. These subsections talk about the outcomes of the comparison research.

4.1 The effect of spring stiffness (Ks) and gap along Z-axis (Gz) on energy harvesting with varying velocity

In open-channel flows, the highest velocity is found below the free surface in comparison to the secondary currents. It is well known that the cross-sectional velocity of turbulent flow in open channels is not spread evenly. The existence of free surfaces and frictional resistance throughout the channel's perimeter is what causes this non-uniformity {Yang, 2004 #64}.

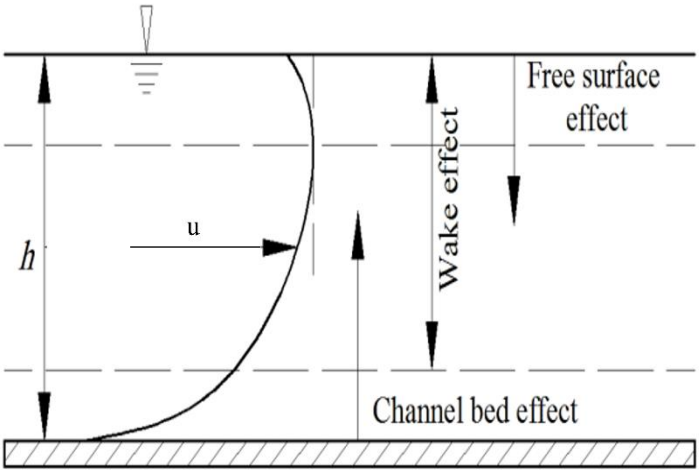

Figure 4.1: Velocity Distribution in Open Channel

In next sub-Sections, we will discuss thoroughly about different flexibly mounted piezoelectric eels and how it effects the flapping frequency, ratio of amplitude to length of

flag and power output. Different spring stiffness are used to study their behavior in wake region and changing the mount position for velocity distribution.

4.1.1 Results at Ks=0.005 N/mm (Frequency, A/L, Power)

After postprocessing of data, different values of frequency, amplitude, and power was observed, according to which Maximum values of frequency = 0.0633, ratio of amplitude to length= 1.108 and power =7.2543 uW were recorded at G_z =6 and maximum of velocity= 0.36m/s as shown in graphs in figure 4.2 and 4.3 below,

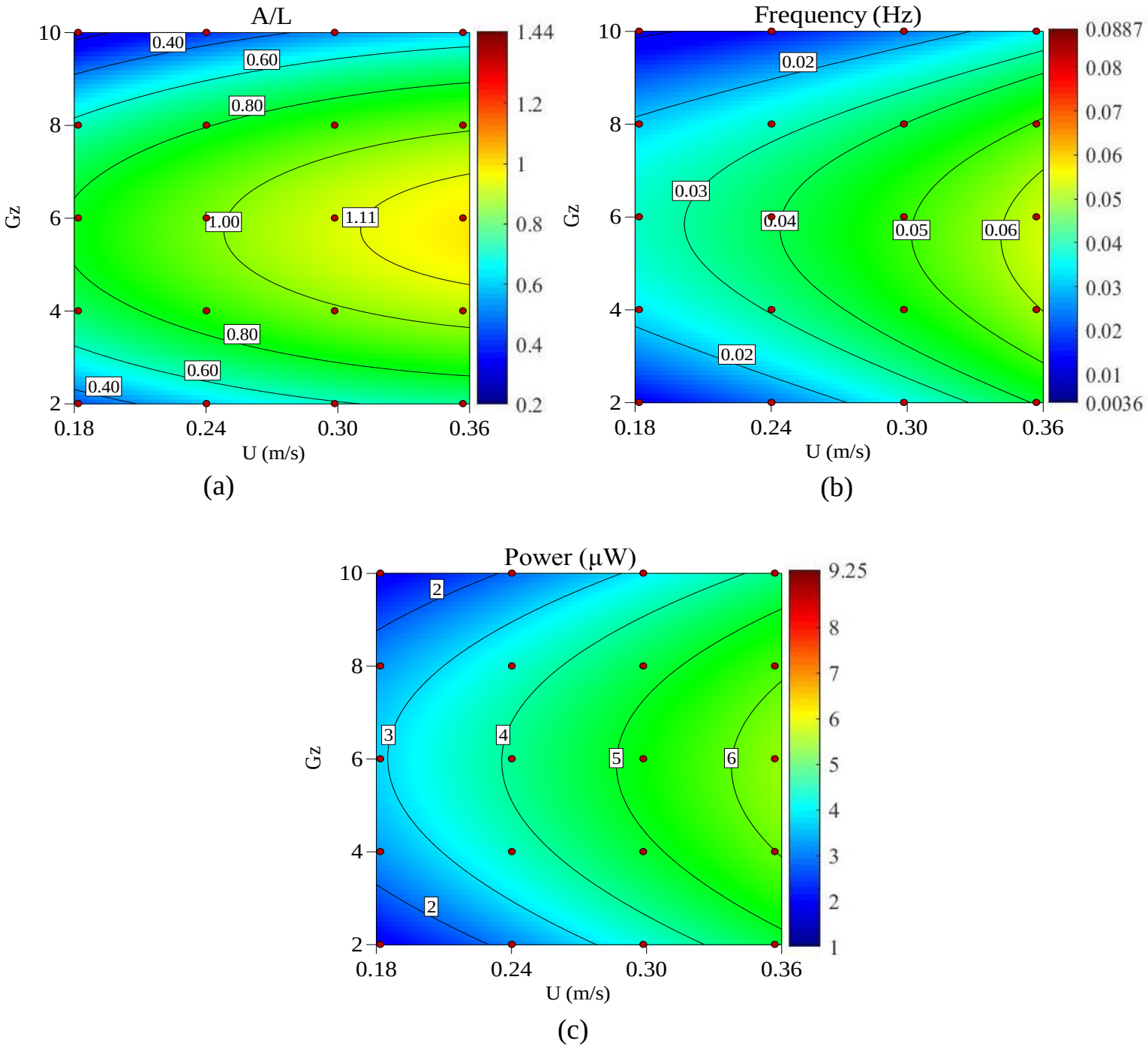

Figure 4.2: Results at K_s =0.005 N/mm (a) Harvested power (µW), (b) frequency, and (c) maximum amplitude per unit length.

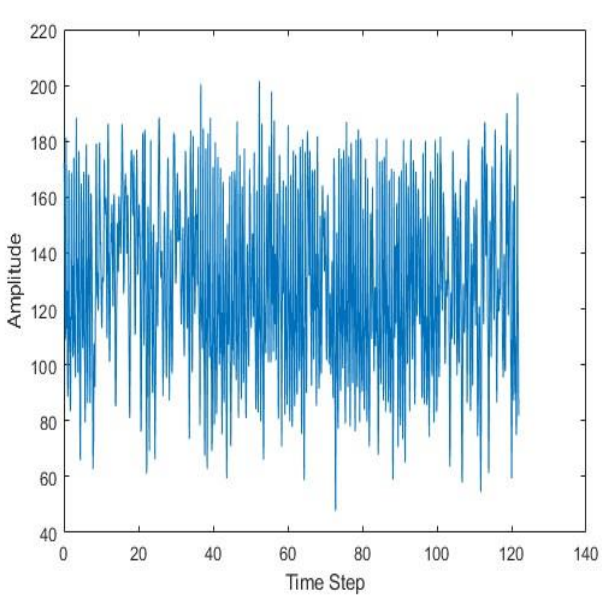

(a)

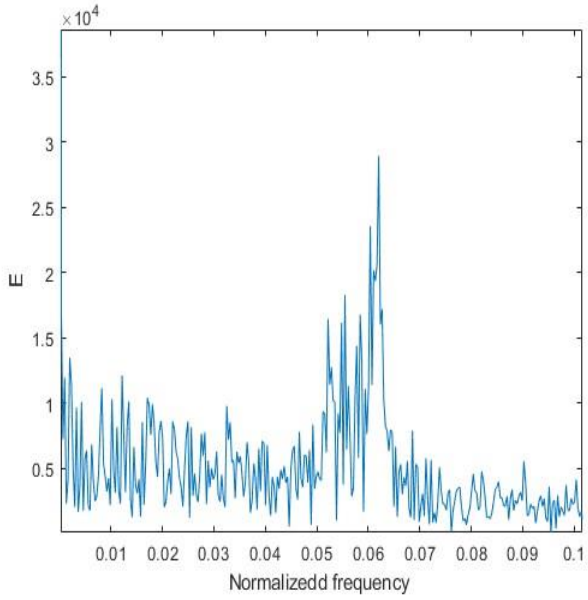

(b)

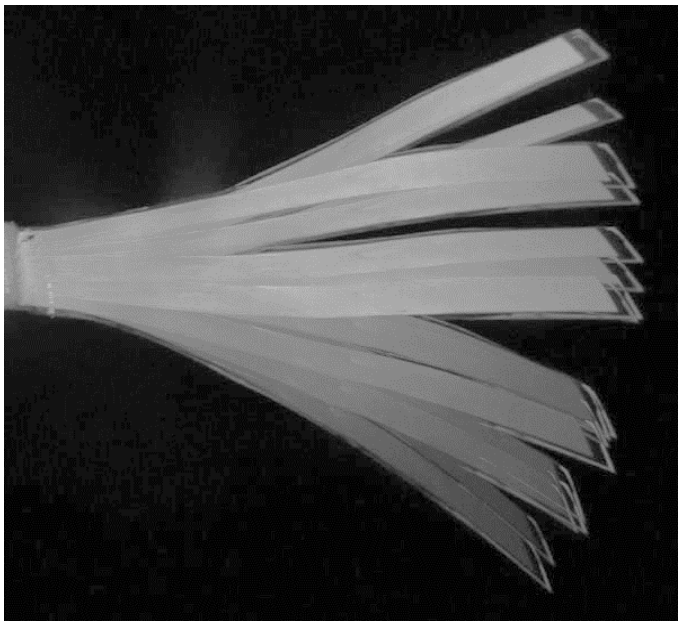

(c)

Fig**ure 4.3:** Maximum Values for Ks =0.005 N/mm (a) Amplitude of trailing edge as a function of time (b) Normalized frequency and, (c) Stroboscopic behavior of trailing edge of eel.

Minimum values of values of frequency = 0.0036, ratio of amplitude to length= 0.2432 and power =1.2041 uW were at G_z =10 i.e., at bottom level and velocity=0.18m/s as shown in figure 4.4. when we moved from bottom to top of cylinder i.e., G_z = 10 to 2,

maximum results were recorded below the free stream surface of open flow channel at $G_z = 4$ and 6 due to maximum velocity observed there because of Velocity dip and secondary currents. In this case least value of output power is observed, it is because velocity is set to minimum 0.18m/s also it is comparatively less at bottom of channel and increase gradually when we move from bottom to top. As the Spring stiffness, position of eel and velocity directly effects the flapping frequency and amplitude, hence we get minimum value of output power at specified position and velocity.

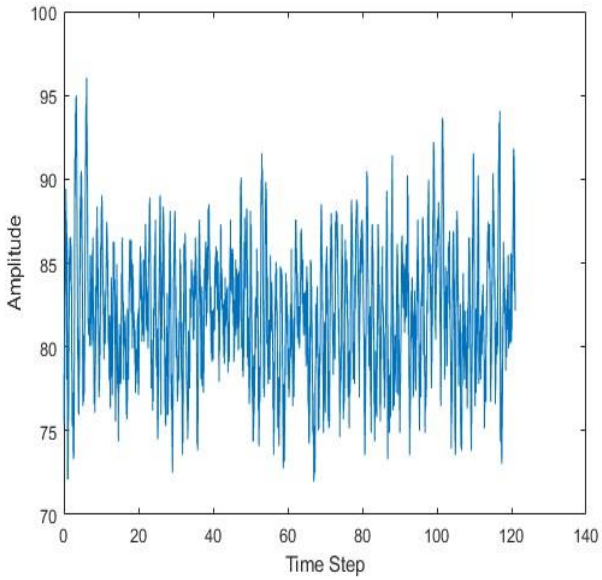

(a)

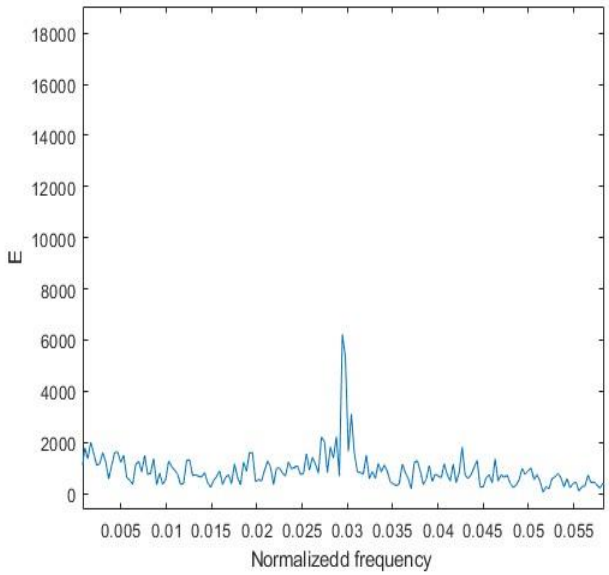

(b)

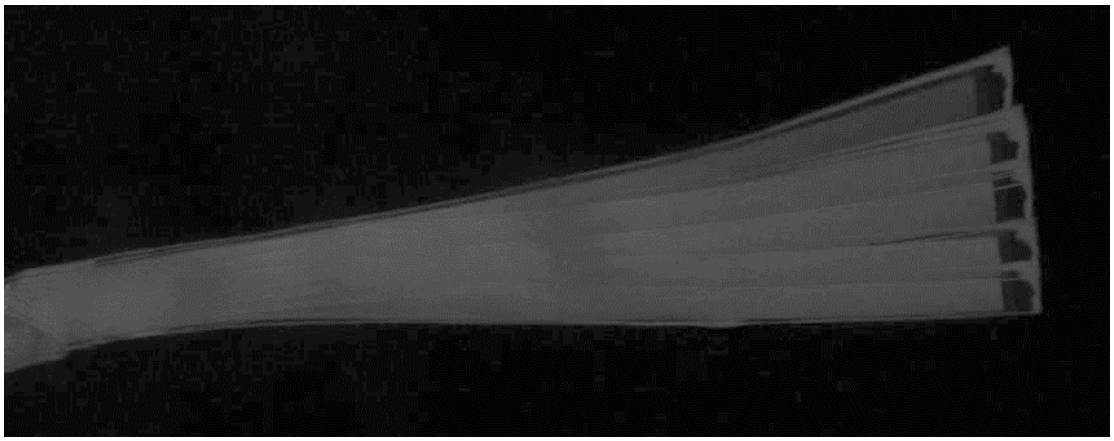

(c)

Figure 4.4: Minimum Values for Ks =0.005 N/mm (a) Amplitude of trailing edge as a function of time (b) Normalized frequency and, (c) Stroboscopic behavior of trailing edge of eel.

4.1.2 Results at Ks=0.023 N/mm (Frequency, A/L, Power)

After postprocessing of data, different values of frequency, amplitude, and power was observed, according to which Maximum values of frequency = 0.07522, ratio of amplitude to length= 1.1824 and power =8.5198 uW were recorded at G_z =6 and maximum of velocity= 0.36m/s as shown in graphs in figure 4.5 and 4.6 below,

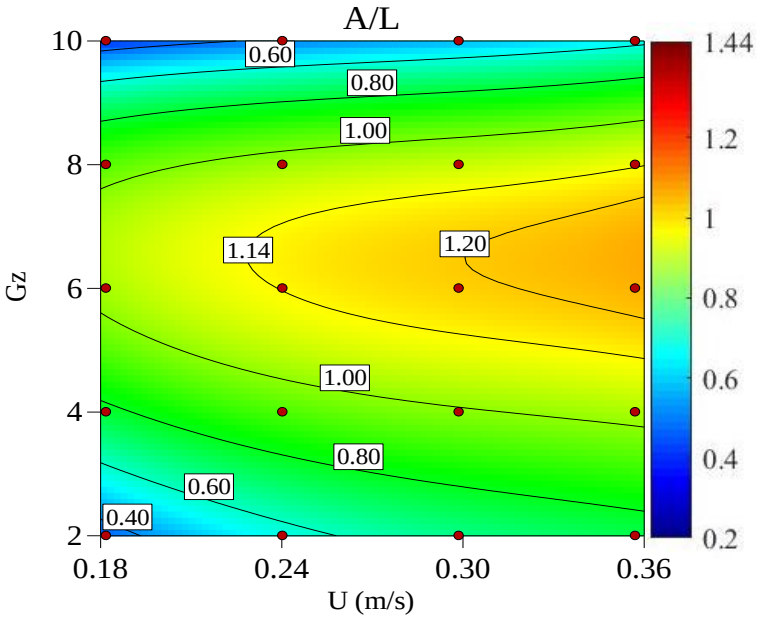

(a)

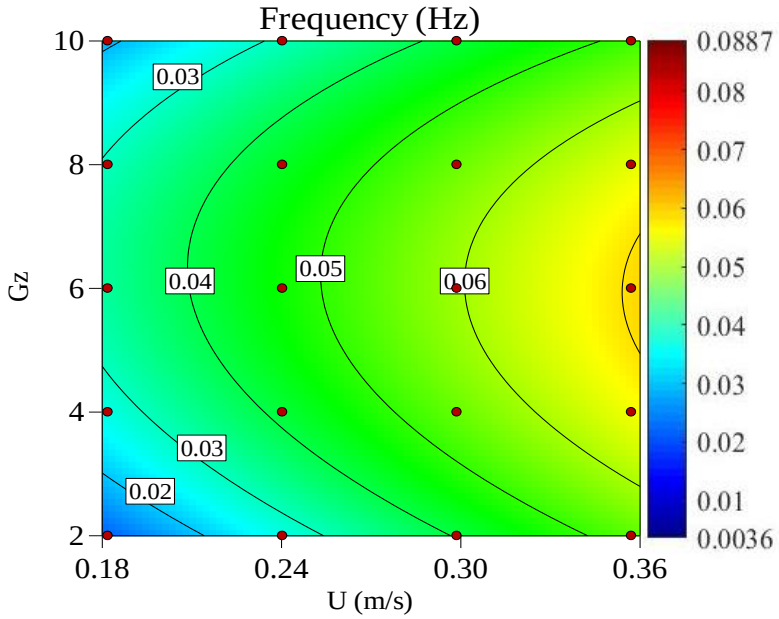

(b)

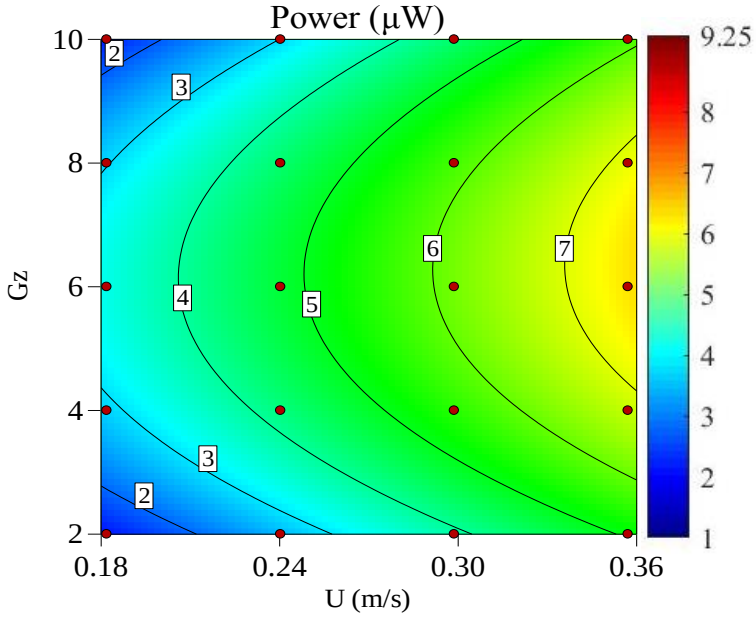

(c)

Figure 4.5: Results at K_s =0.023 N/mm (a) Harvested power (μW), (b) frequency, and (c) maximum amplitude per unit length.

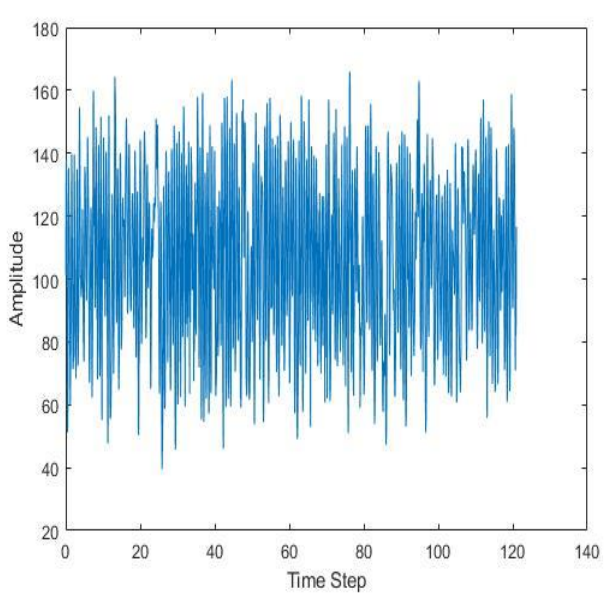

(a)

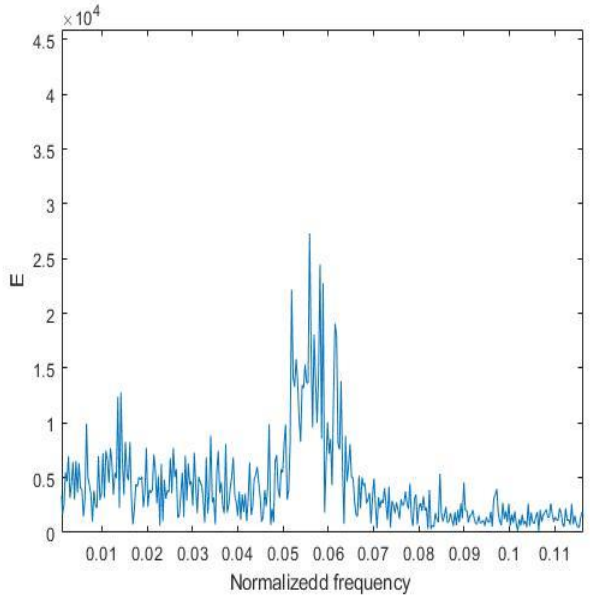

(b)

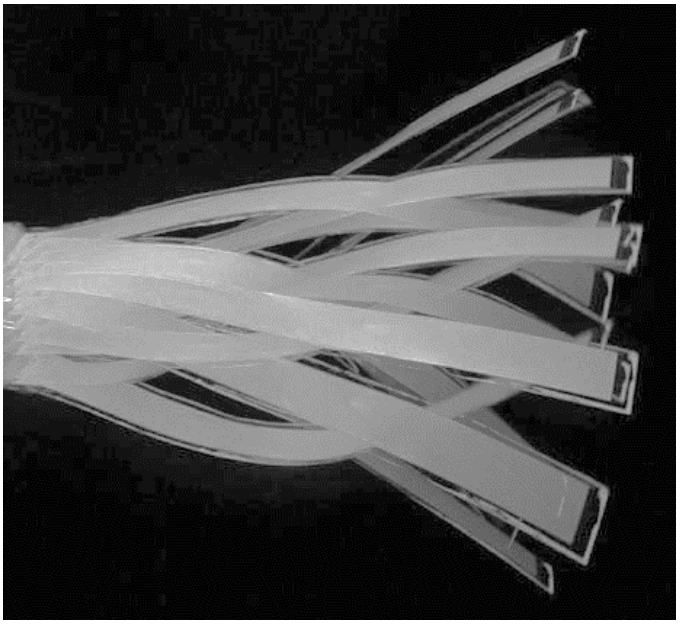

(c)

Figure 4.6: Maximum Values for K_s =0.023 N/mm (a) Amplitude of trailing edge as a function of time (b) Normalized frequency and, (c) Stroboscopic behavior of trailing edge of eel.

Minimum values of values of frequency = 0.0165, ratio of amplitude to length= 0.3144 and power =2.1041 uW were at G_z =10 i.e., at bottom level and velocity=0.18m/s as shown in figure 4.7. when we moved from bottom to top of cylinder i.e., G_z = 10 to 2, maximum results were recorded below the free stream surface of open flow channel at G_z = 4 and 6 just because of Velocity dip and secondary currents.

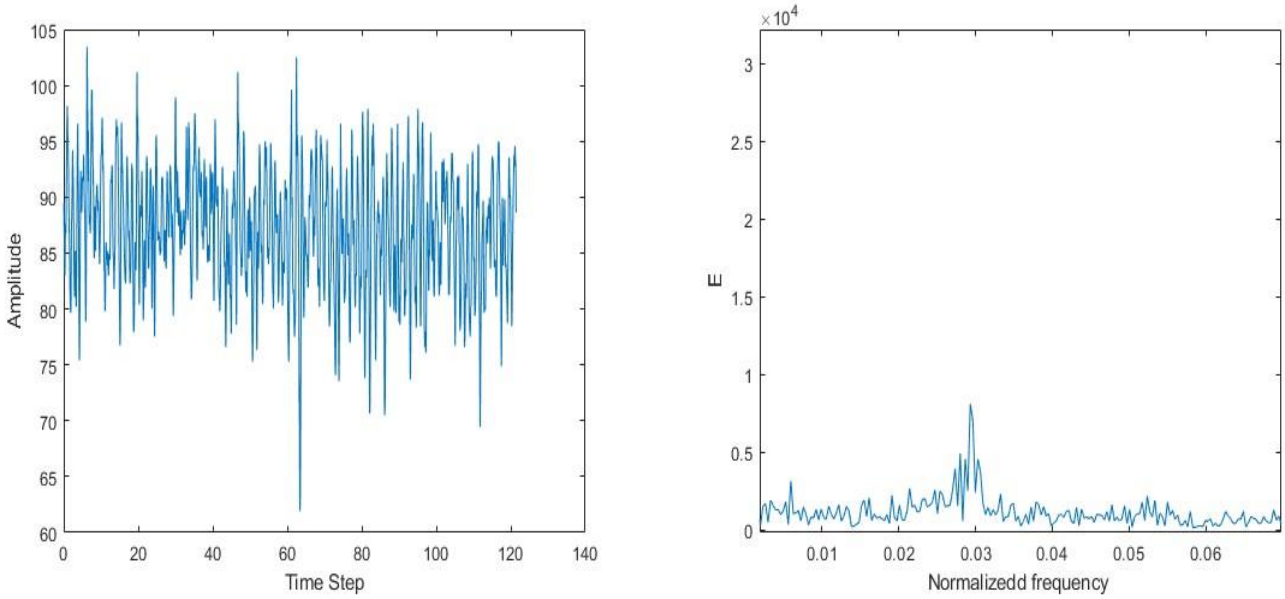

(a) (b)

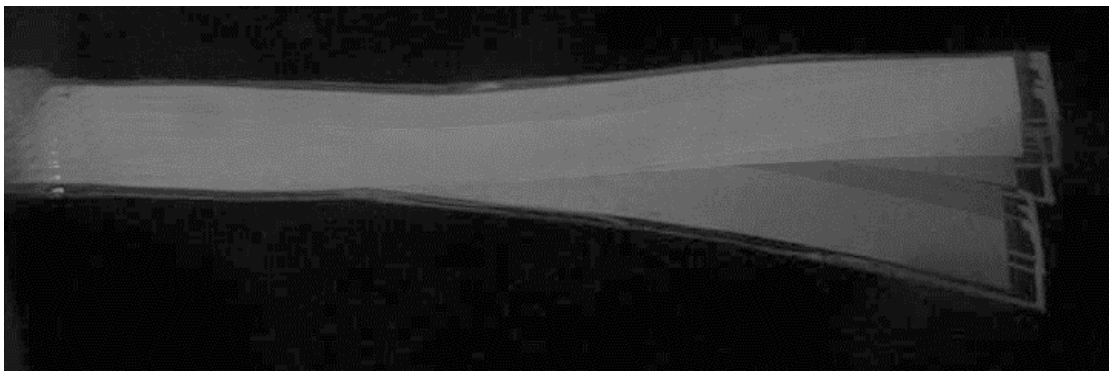

(c)

Figure 4.7: Minimum Values for K_s =0.023 N/mm (a) Amplitude of trailing edge as a function of time (b) Normalized frequency and, (c) Stroboscopic behavior of trailing edge of eel.

4.1.3 Results at Ks=0.027 *N/mm* (Frequency, A/L, Power)

After postprocessing of data, different values of frequency, amplitude, and power was observed, according to which Maximum values of frequency = 0.0801, ratio of amplitude to length= 1.2251 and power =8.6558 uW were recorded at G_z =6 and maximum of velocity= 0.36m/s as shown in graphs in figure 4.8 and 4.9 below,

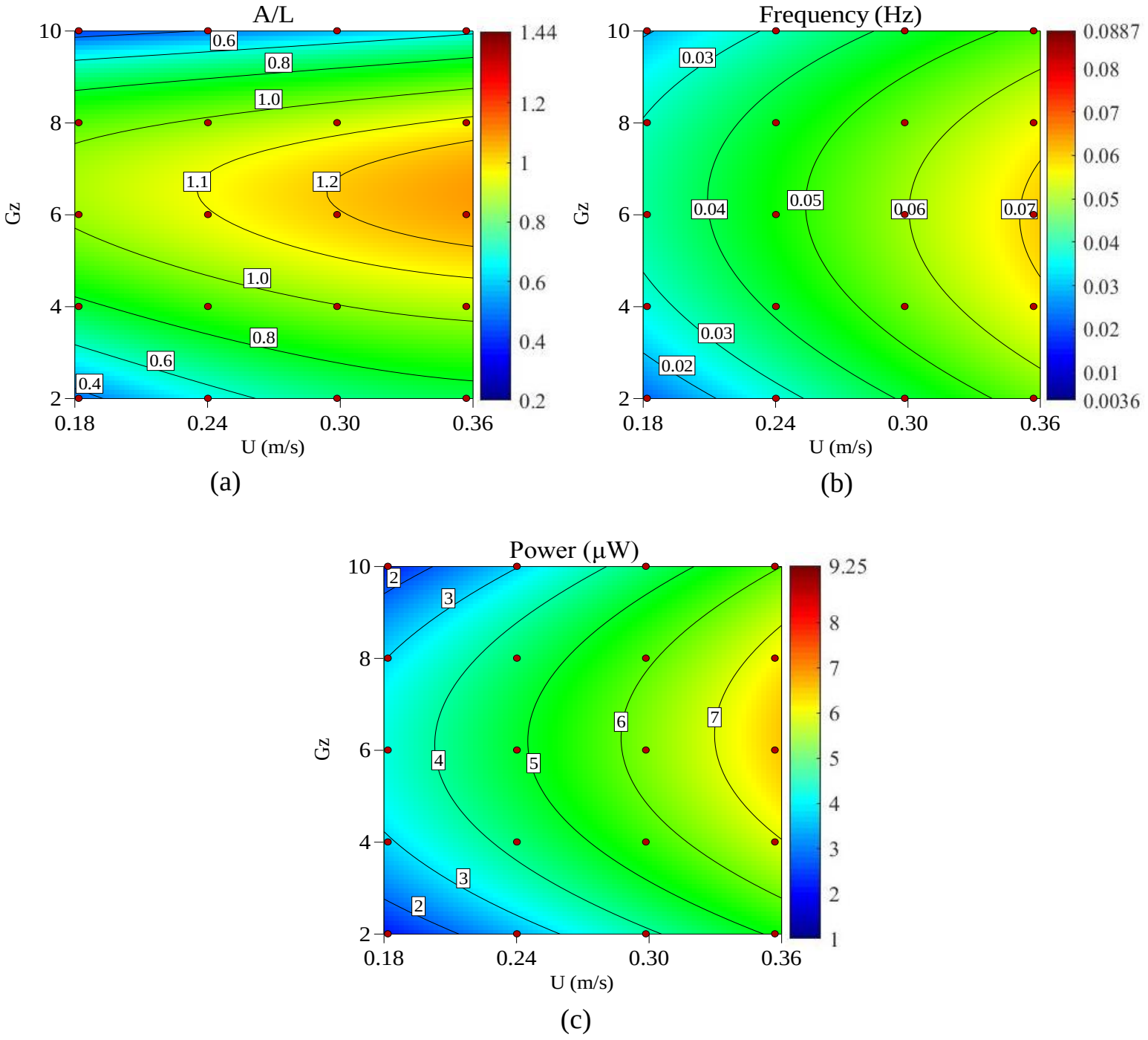

Figure 4.8: Results at K_s =0.027 N/mm (a) Harvested power (µW), (b) frequency, and (c) maximum amplitude per unit length.

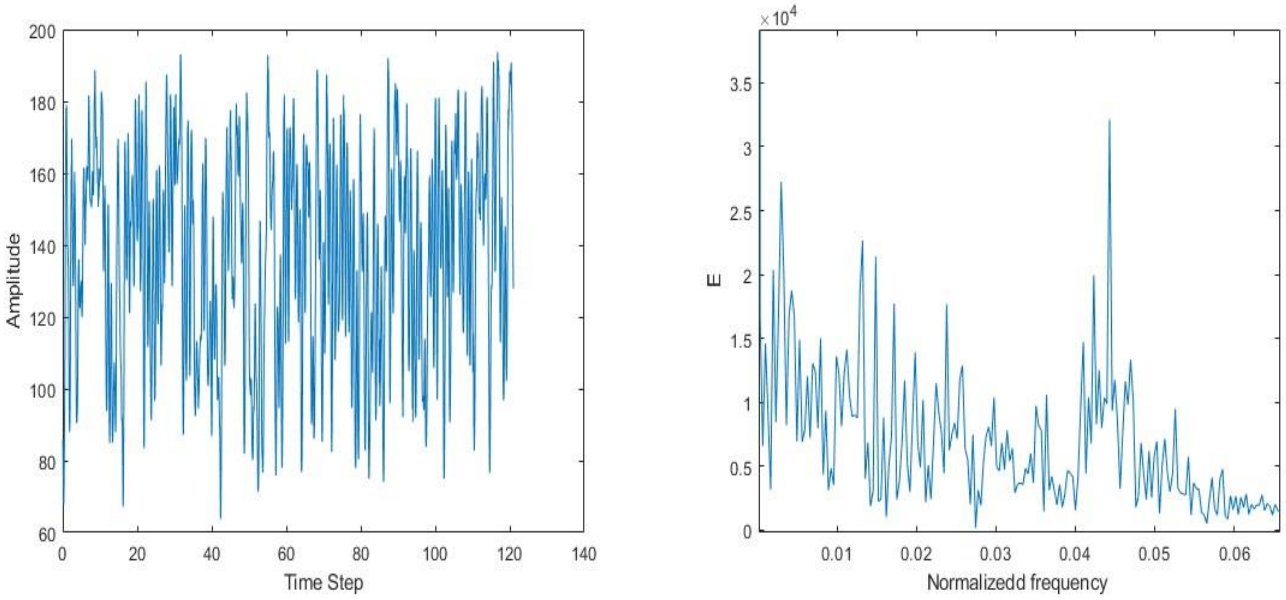

(a) (b)

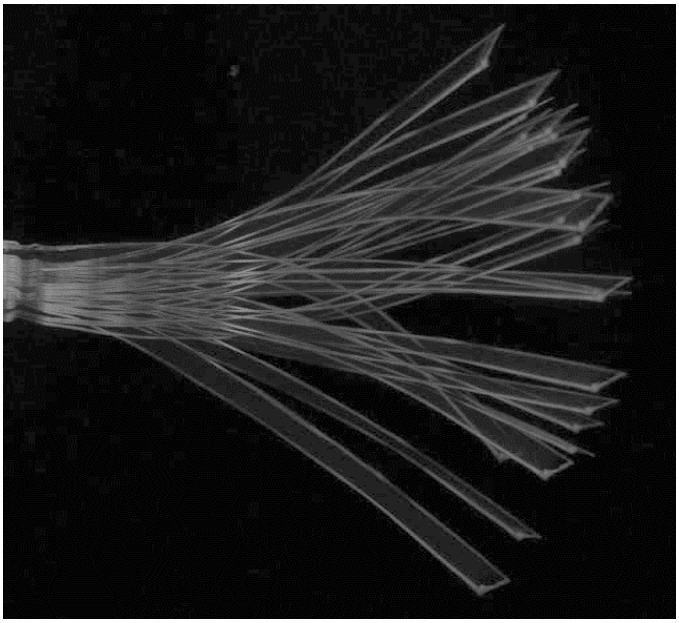

(c)

Figure 4.9: Maximum Values for K_s =0.027 N/mm (a) Amplitude of trailing edge as a function of time (b) Normalized frequency and, (c) Stroboscopic behavior of trailing edge of eel.

Minimum values of values of frequency = 0.0165, ratio of amplitude to length= 0.3144 and power =2.1041 uW were at G_z =10 i.e., at bottom level and velocity=0.18m/s as shown in figure 4.10. when we moved from bottom to top of cylinder i.e., G_z = 10 to 2, maximum results were recorded below the free stream surface of open flow channel at G_z = 4 and 6 just because of Velocity dip and secondary currents.

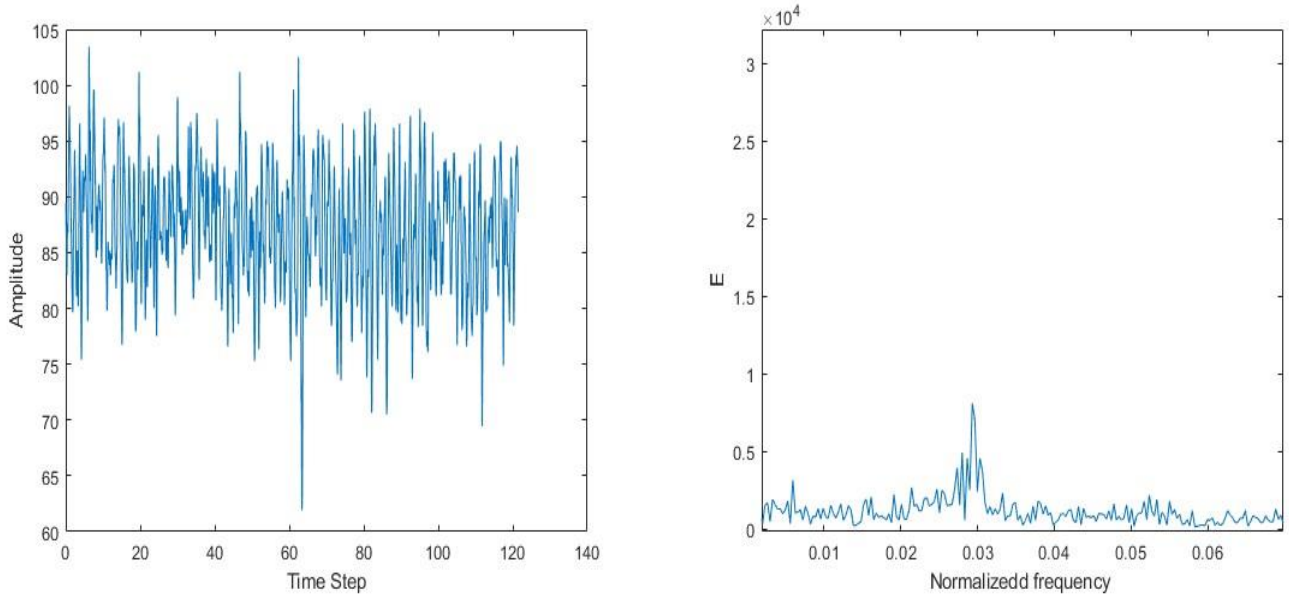

(a) (b)

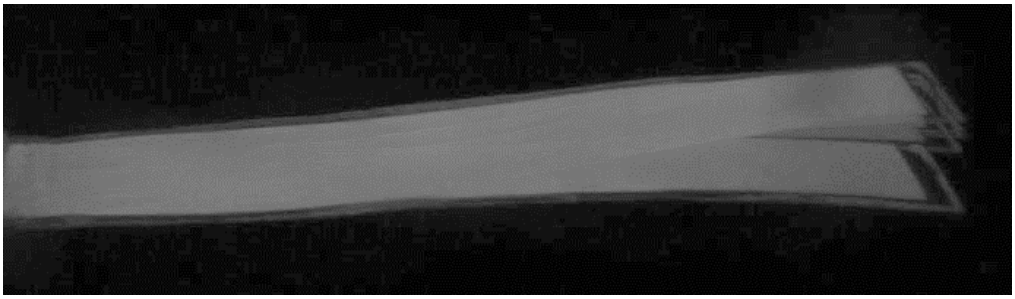

(c)

Figure 4.10: Minimum Values for K_s =0.027 N/mm (a) Amplitude of trailing edge as a function of time (b) Normalized frequency and, (c) Stroboscopic behavior of trailing edge of eel.

4.1.4 Results at Ks=0.05 *N/mm* (Frequency, A/L, Power)

After postprocessing of data, different values of frequency, amplitude, and power was observed, according to which Maximum values of frequency = 0.08023, ratio of amplitude to length= 1.2873 and power =8.8558 uW were recorded at G_z =6 and maximum of velocity= 0.36m/s as shown in graphs in figure 4.11 and 4.12 below,

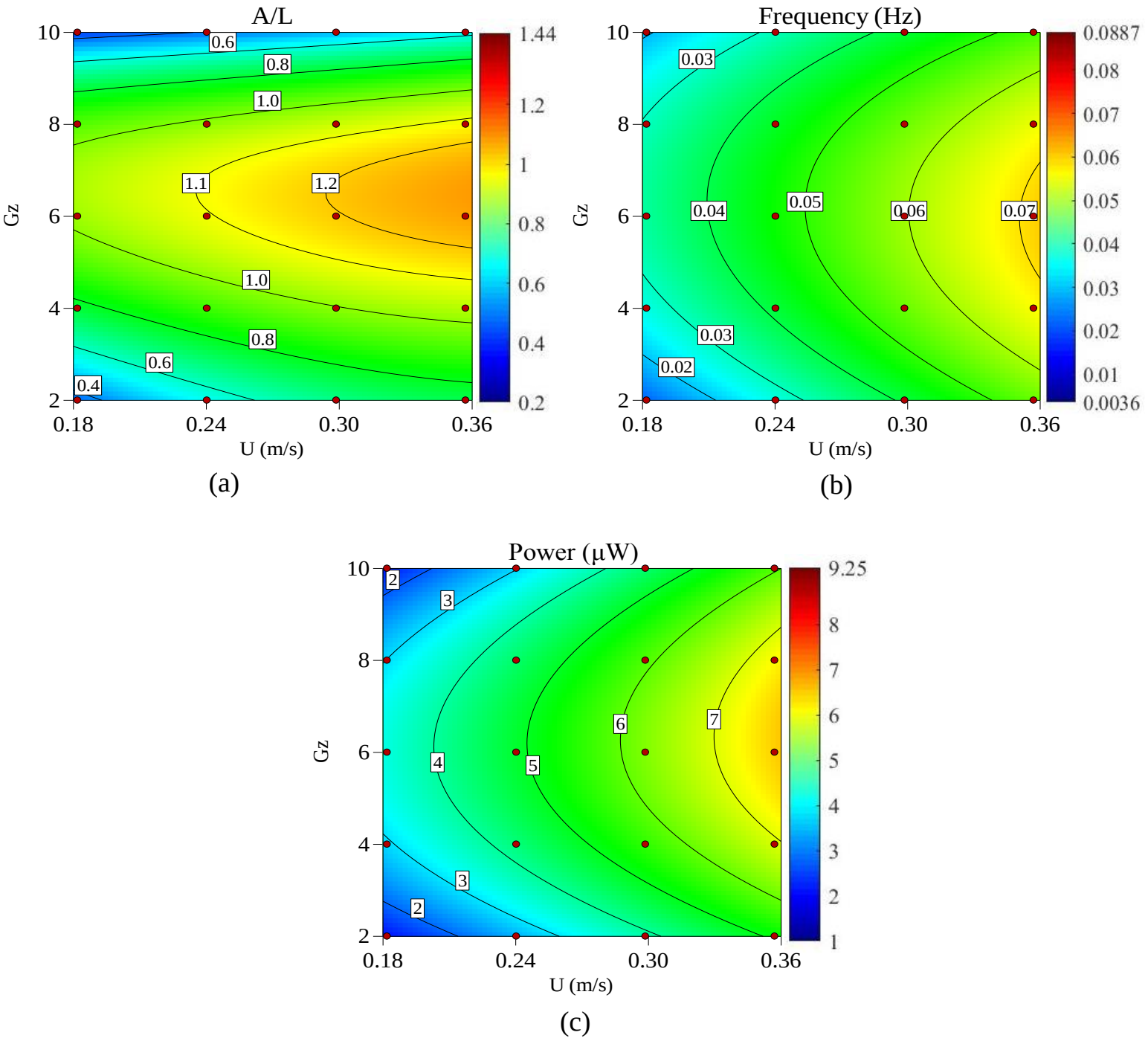

Figure 4.11: Results at K_s =0.05 N/mm (a) Harvested power (µW), (b) frequency, and (c) maximum amplitude per unit length.

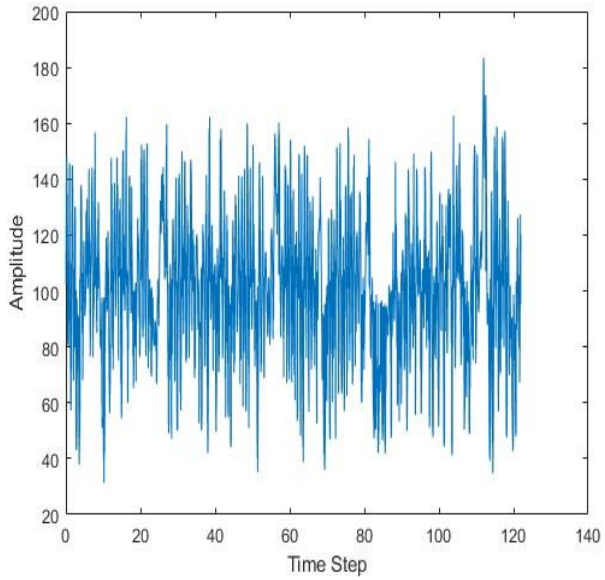

(a)

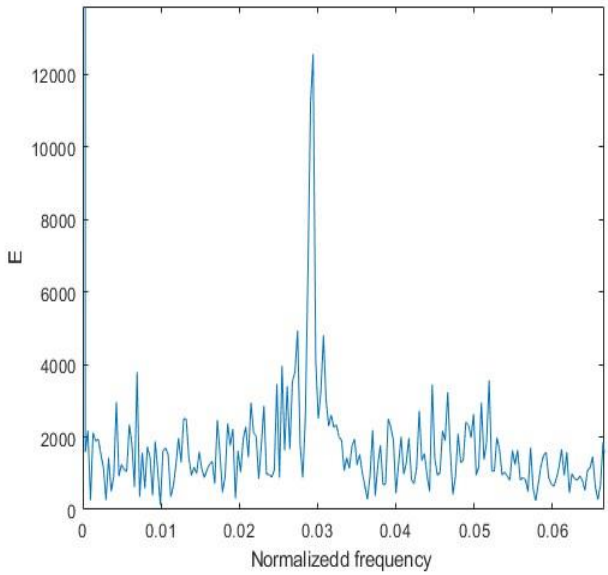

(b)

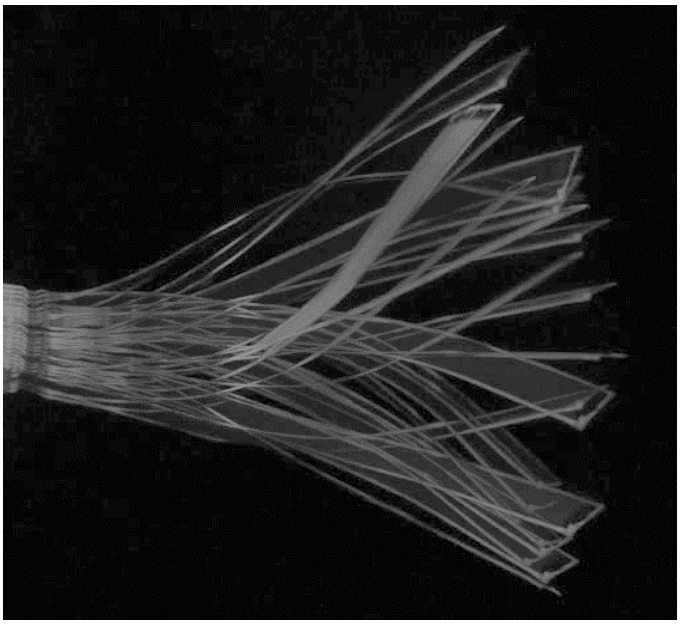

(c)

Figure 4.12: Maximum Values for K_s =0.05 N/mm (a) Amplitude of trailing edge as a function of time (b) Normalized frequency and, (c) Stroboscopic behavior of trailing edge of eel.

Minimum values of values of frequency = 0.01416, ratio of amplitude to length= 0.3268 and power =2.1741 uW were at G_z =10 i.e., at bottom level and velocity=0.18m/s as shown in figure 4.13. when we moved from bottom to top of cylinder i.e., G_z = 10 to 2, maximum results were recorded below the free stream surface of open flow channel at G_z = 4 and 6 just because of Velocity dip and secondary currents.

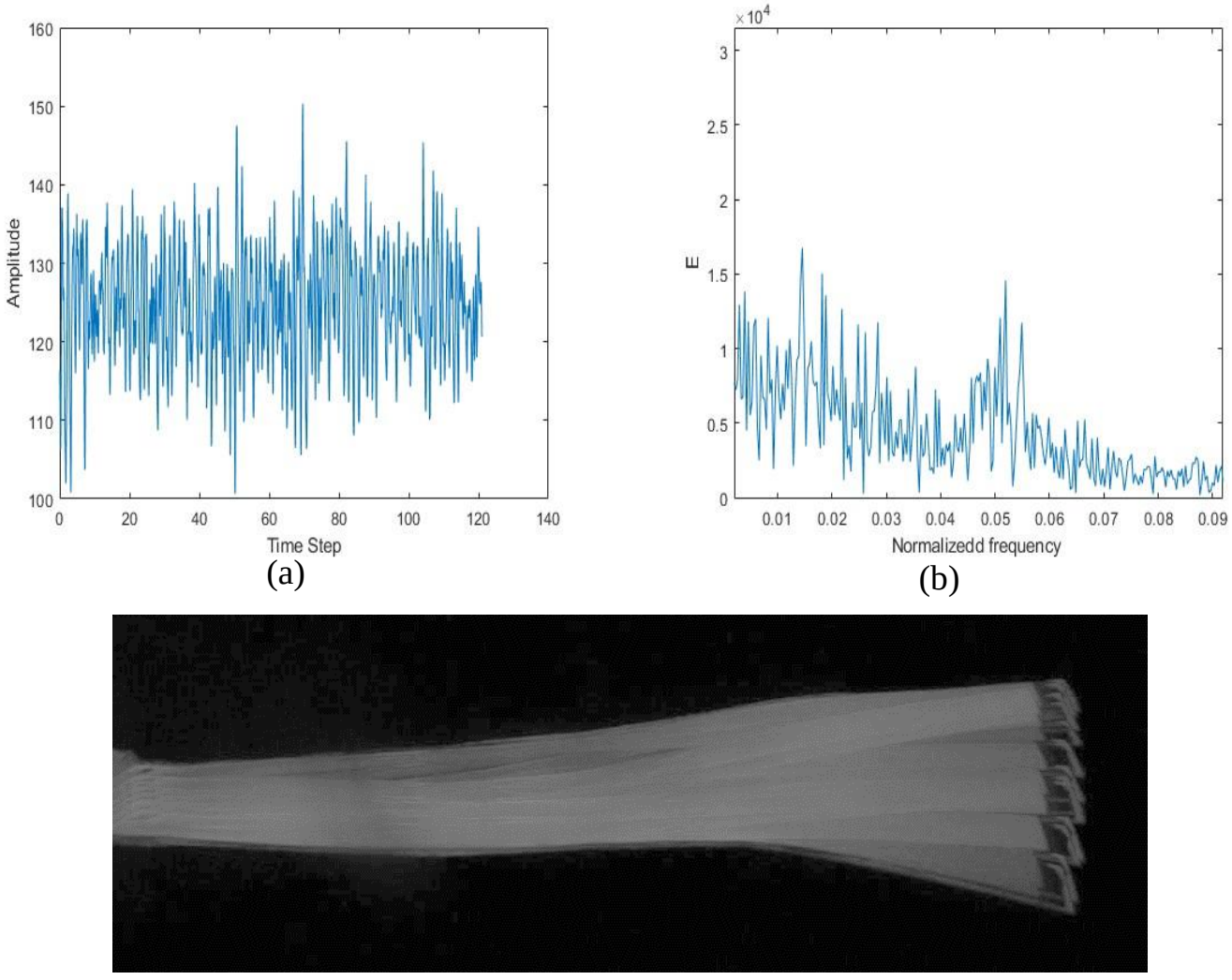

(a) (b)

(c)

Figure 4.13: Minimum Values for K_s =0.05 N/mm (a) Amplitude of trailing edge as a function of time (b) Normalized frequency and, (c) Stroboscopic behavior of trailing edge of eel.

4.1.5 Results at Ks=0.07 *N/mm* (Frequency, A/L, Power)

After postprocessing of data, different values of frequency, amplitude, and power was observed, according to which Maximum values of frequency = 0.0887, ratio of amplitude to length= 1.4361 and power =9.2502 uW were recorded at G_z =6 and maximum of velocity= 0.36m/s as shown in graphs in figure 4.14 and 4.15 below,

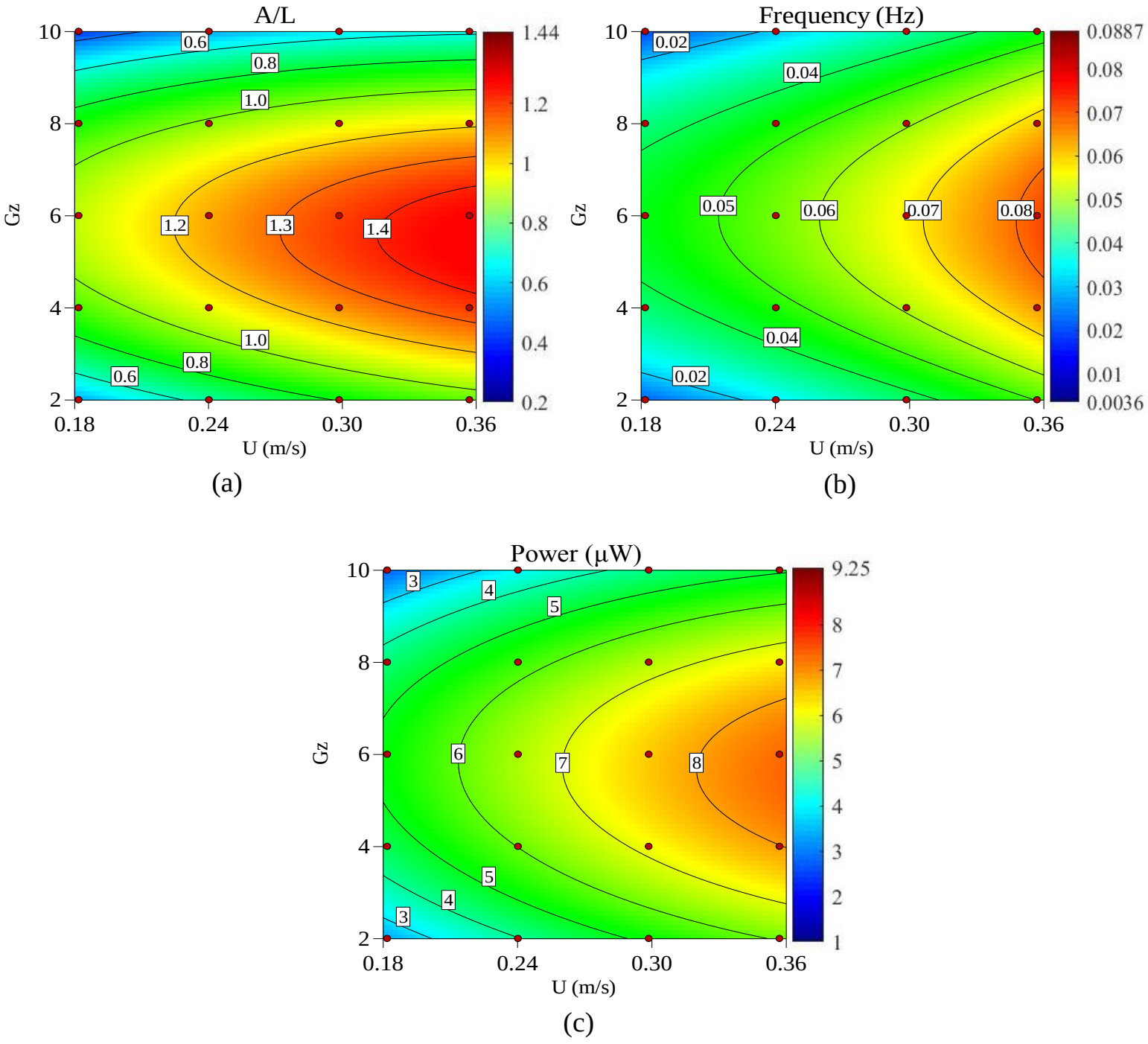

Figure 4.14: Results at K_s =0.07 N/mm (a) Harvested power (µW), (b) frequency, and (c) maximum amplitude per unit length.

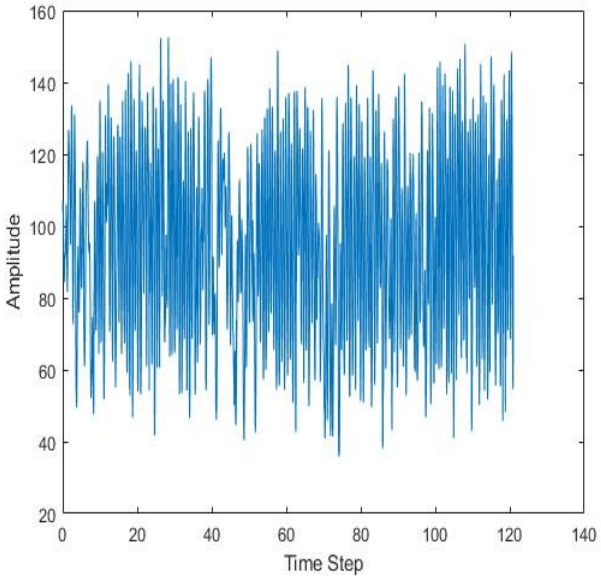

(a)

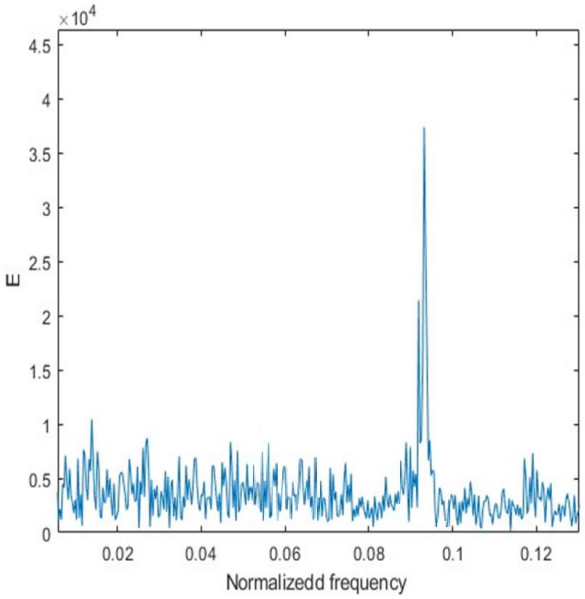

(b)

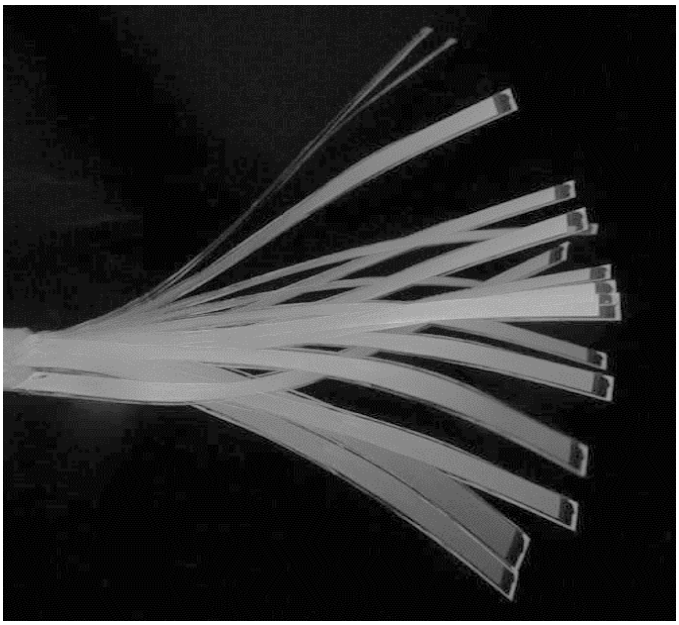

(c)

Figure 4.15: Maximum Values for K_s =0.07 N/mm (a) Amplitude of trailing edge as a function of time (b) Normalized frequency and, (c) Stroboscopic behavior of trailing edge of eel.

Minimum values of values of frequency = 0.009154, ratio of amplitude to length= 0.3802 and power =2.2159 uW were at G_z =10 i.e., at bottom level and velocity=0.18m/s as shown in figure 4.16. when we moved from bottom to top of cylinder i.e., G_z = 10 to 2, maximum results were recorded below the free stream surface of open flow channel at G_z = 4 and 6 just because of Velocity dip and secondary currents.

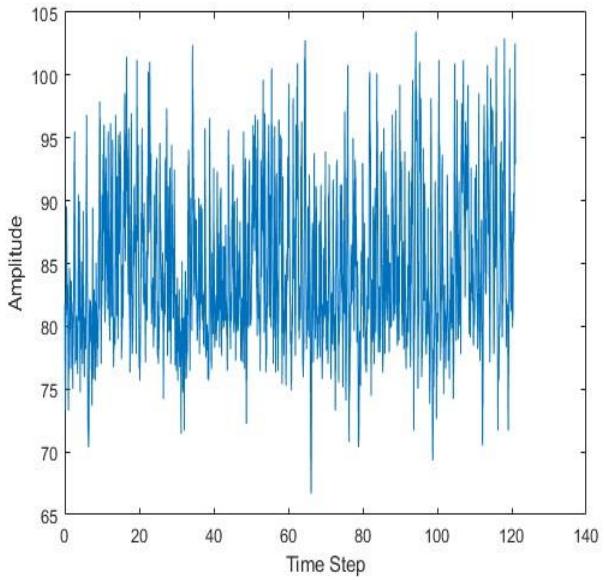

(a)

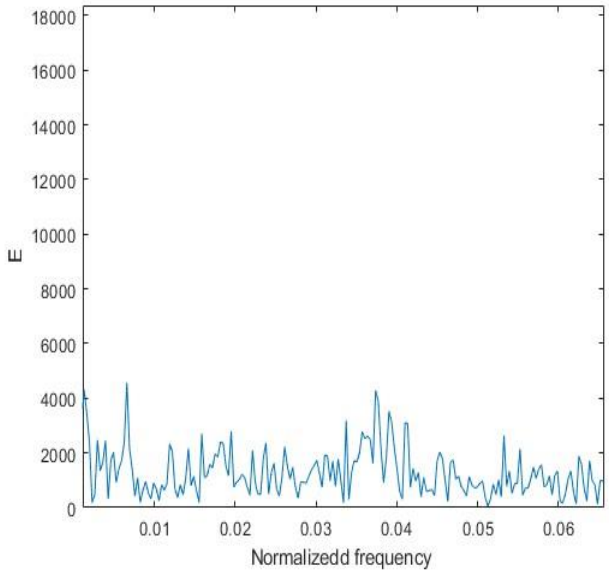

(b)

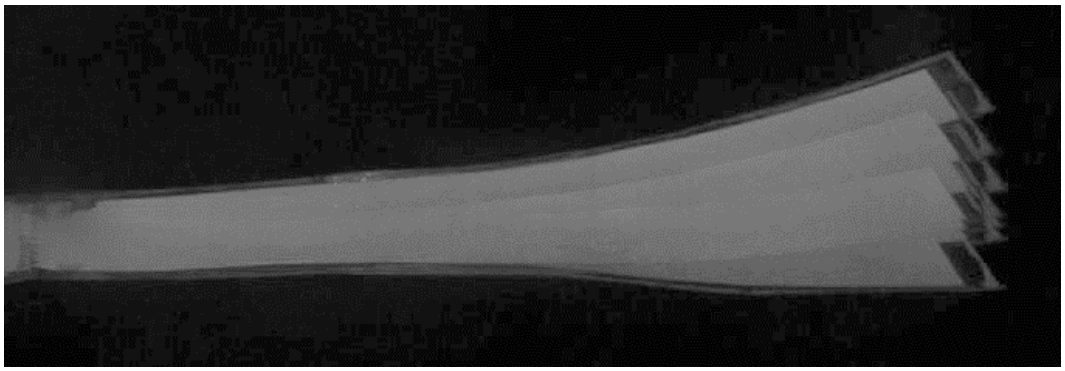

(c)

Figure 4.16: Minimum Values for Ks = 0.07 N/mm (a) Amplitude of trailing edge as a function of time (b) Normalized frequency and, (c) Stroboscopic behavior of trailing edge of eel.

4.2 Comparative study of different spring stiffness (Ks) with velocity (U) at Gz=6

In previous sub sections we had studied that, how the Spring Stiffness (Ks) behave with Gap along Z-axis (Gz) on Energy Harvesting with varying Velocity. From there we have concluded that maximum results were obtained at Gz=6. Now we are considering the results of amplitude to length ratio, frequency, and power for different spring stiffness with varying velocity at Gz=6 which are summarized below in table 6.

Table 6: Summarized results of A/L, frequency, and power

K_s (N/mm)	U(m/s)	A/L	F(Hz)	P(μW)
0.005	0.18	0.8647	0.0301	2.2041
	0.24	0.9884	0.0392	3.2159
	0.30	1.0187	0.0508	4.0543
	0.36	1.0480	0.0620	4.6543
0.023	0.18	0.9380	0.0305	2.2041
	0.24	1.0848	0.0525	3.2159
	0.30	1.0954	0.0682	4.2580
	0.36	1.1512	0.0802	5.9080
0.027	0.18	0.9932	0.0305	2.2041
	0.24	1.0286	0.0545	3.2159
	0.30	1.1839	0.0682	5.5798
	0.36	1.2251	0.0802	6.4580
0.05	0.18	1.1558	0.0444	3.1041
	0.24	1.2206	0.0598	5.1588
	0.30	1.2251	0.0695	6.3798
	0.36	1.2873	0.0752	7.2798
0.07	0.18	1.1499	0.0444	4.1809
	0.24	1.1832	0.0598	5.2959
	0.30	1.2836	0.0795	7.1780
	0.36	1.4361	0.0887	9.2508

4.3 The effect of Spring Stiffness on Energy Harvesting with varying velocity at Gz=6

Results from above table 6; are graphically represented in this sub section, which shows that with increasing the spring stiffness from 0.005 to 0.07(N/mm) and velocity U(m/s) we are obtaining the increasing values of amplitude to length ratio (A/L), Frequency (Hz) and power (uW). These parameters ultimately increase the output voltage of system and hence maximized power (uW). Contours of A/L, frequency, and power for different spring stiffness with respect to velocity are shown below in figure 4.20.

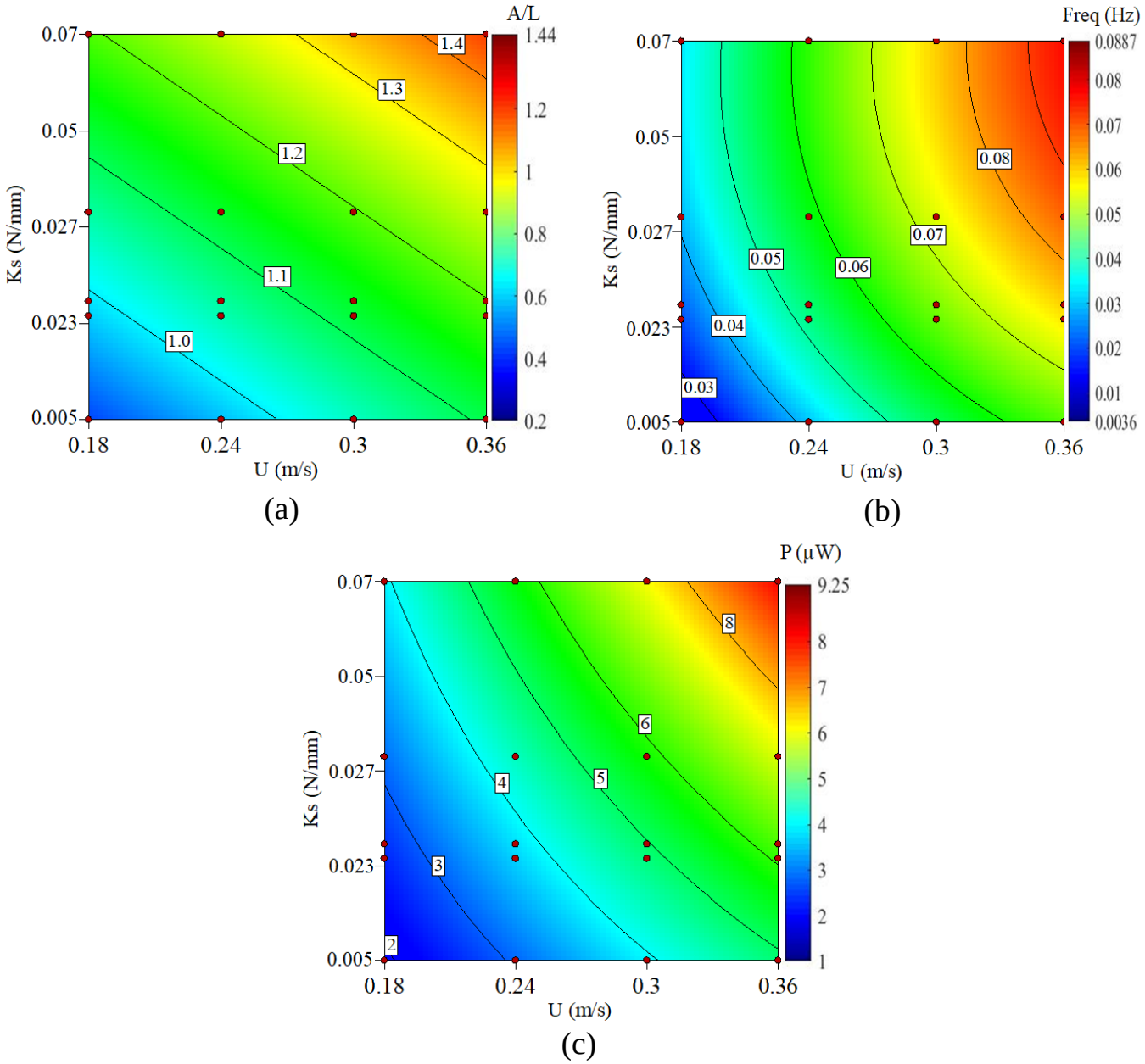

Figure 4.17: Contours for Ks (N/mm) vs U (m/s) at Gz=6 (a) maximum amplitude per unit length, (b) frequency (Hz), and (c) Harvested power (µW).

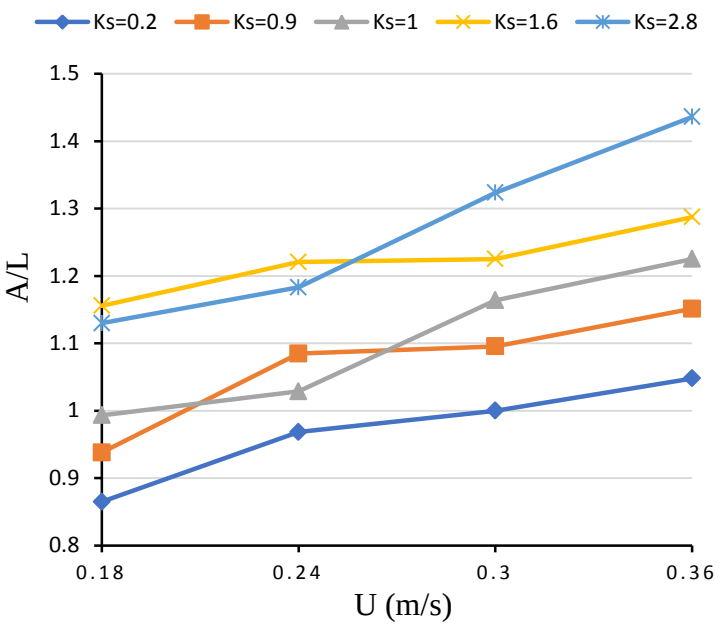

(a)

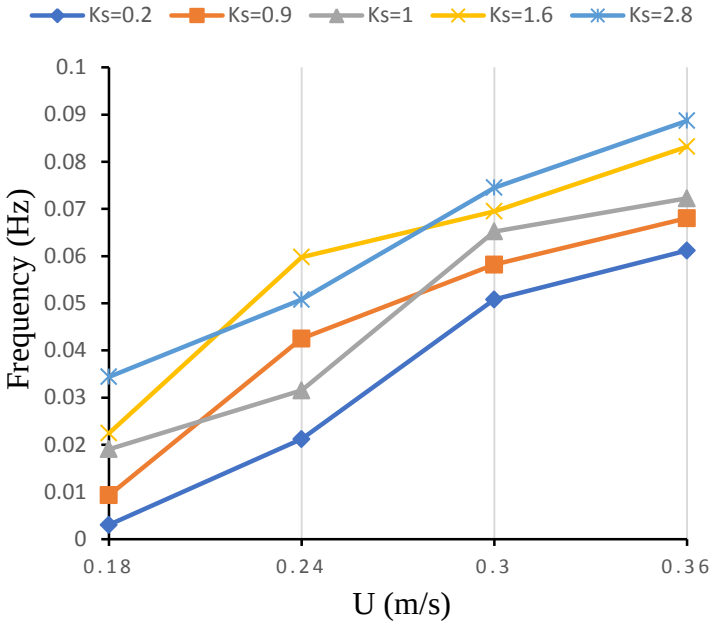

(b)

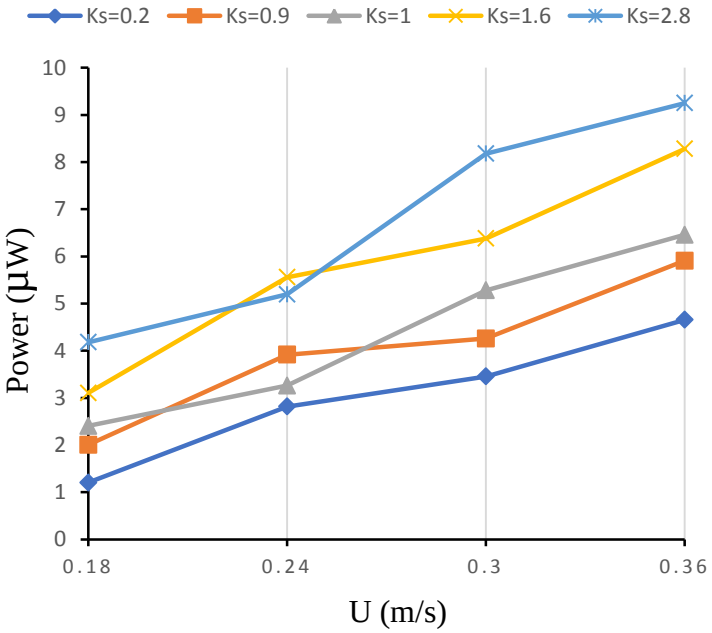

(c)

Figure 4.18: Line plots to elaborate the trends followed by Ks (N/mm) for (a) A/L, (b) Frequency and (c) Power

Chapter 5: Conclusions

In this research study, the energy harvesting by using flexibly mounted piezoelectric eel in wake of inverted c-shape cylinders is investigated. Springs having different stiffness are used to mount piezoelectric eel, position of flexibly mounted pvdf eel is varied along the vertical length of cylinder in z-axis, and velocity is increased gradually from 0.18 to 0.36 m/s. Investigations on the behavior of a piezoelectric flag focus on its RMS voltage, flapping frequency, and peak-to-peak oscillation amplitude. The quantity and rate of strain applied to the piezoelectric eel directly affect the buildup of electrical charges on its terminals, which leads to the harvesting of power. Consequently, the maximum power is harvested where the frequency and amplitude of flapping are higher.

It is concluded from the research that by increasing the spring stiffness i.e., Ks=0.07 and velocity of flow equal to 0.36m/s results in highest frequency of 0.0887Hz, amplitude to length ratio of 1.4361 and consequently maximum amount of output power which is 9.25uW. all these maximum results are obtained at G_z = 6, which is somewhat below the free stream surface of water, it is because the maximum velocity is always obtained just below the free surface of water in open channel flow because of velocity dip phenomenon and movement of secondary currents in transverse direction at top surface of water. It is also necessary to mention that minimum values were obtained at bottom level of flow at G_z = 10, lower spring stiffness i.e., Ks=0.005 and lowest flow velocity of 0.18 m/s.

All results of current study are compared and analyzed with recently published work of different authors. Handsome amount of increment is observed in values of frequency, amplitude to length ratio and output power. Which is as follows,

- U. Latif et al. 2021 Results of circular cylinder (non-pivoted) are taken as reference values i.e., flapping frequency is equal to 0.0706Hz, amplitude to length ratio is equal to 0.822 and power is equal to 3.460 µW {Latif, 2021 #52}.
- U. Latif et al. 2021 Results of inverted C-shape cylinder (non-pivoted) are compared with circular cylinder(non-pivoted) and there was percentage increase in flapping frequency, amplitude to length ratio and output power is 19.1%, 30.25% and 65.93% respectively {Latif, 2021 #52}.
- Results of current study for inverted C-shape cylinder (Flexibly mounted piezoelectric eel or pivoted eel in which head of eel is also moving instead of fixed) are compared with inverted C-shape cylinder (non-pivoted) mentioned above. While comparing the

results, significant amount of increment is observed in flapping frequency, amplitude to length ratio and output power which is **5.47%, 34.13%** and **61.12%** respectively.

The comparison of flapping frequency, amplitude to length ratio and output power in current study with previous one is described in table 6

Table 7: Comparison of Results

Mechanism	***A/L***	***Freq (Hz)***	***Power (µW)***
U. Latif et al. 2021 Results for Circular (non-pivoted)	0.822	0.0706	3.460
	(Taken as ref value)		
U. Latif et al. 2021 Results for Inverted C-Shaped (non-pivoted)	1.0706	0.0840	5.741
	30.25%↑+	19.1%↑+	65.93%↑+
Current Study Results for inverted C-Shaped (pivoted)	1.4361	0.0887	9.25
	34.13%↑+	**5.47%↑+**	**61.12%↑+**
	Compared with C-Shaped (non-pivoted)		

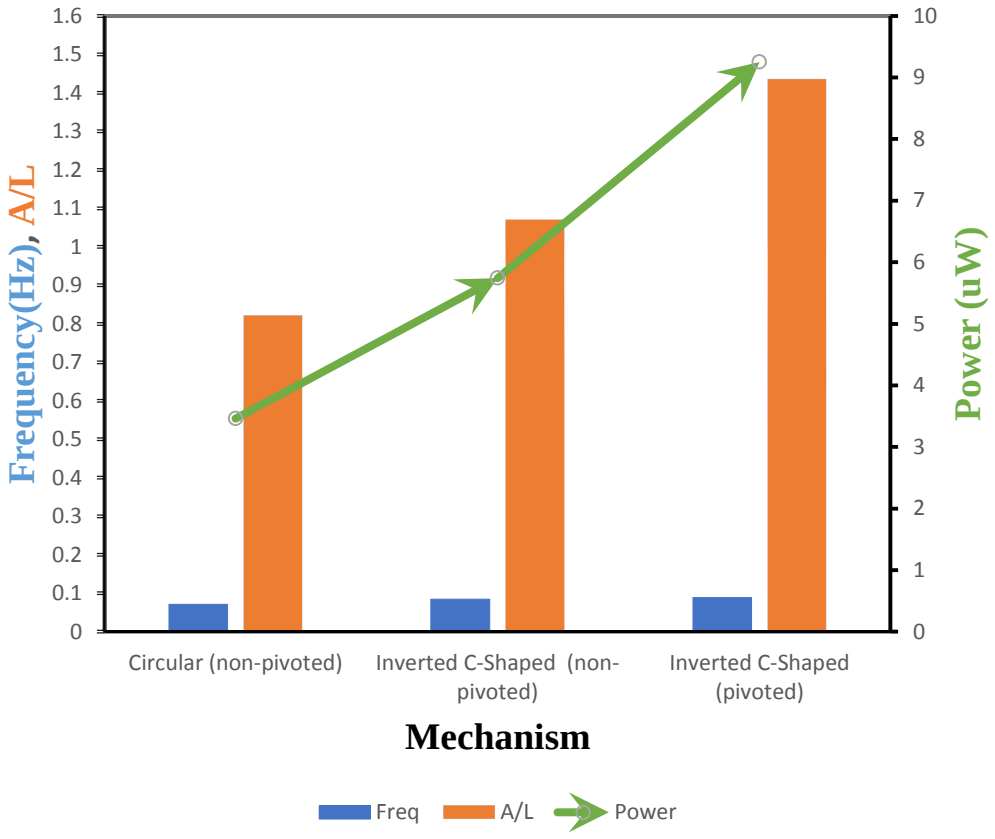

Figure 5.1: Overall Results comparison with published work

Appendix

MATLAB code for data extraction from video to excel file

```
clc;
clear ;
close all;
% Batch Processing
video_files = {dwdwbww.mp4};
vidObj = VideoReader(video_files{1}); %
I = readFrame(vidObj);
[J, rect] = imcrop(I);   % J is image and rect is coor
level=0.1;
Ithresh = im2bw(J,level);
% Batch End
%Converting Vedio to a Array of Vector Frames
for vid = 1:length(video_files)
disp('Working on video')
vidObj = VideoReader(video_files{vid});
tip_pos = zeros(1,2);
cuurentframe = 1;
ss = zeros(size(Ithresh));   % For adding Images
vidObj.CurrentTime = 0.0;
while hasFrame(vidObj)
   F = readFrame(vidObj);
   fprintf('Current Processing Frame:\t %d\n', cuurentframe)
%Converting from RGB to Grayscale and save them in Cell Array
   U = rgb2gray(F);
%Cropping frames to desire Workspace
   Q=imcrop(U, rect); %XY value to crop them in a desired workspace
% Converting Array of Crop Images into Binary Image
    W=Q>25; %threshold to remove unwanted region
   %W = imbinarize(Q);
% Image Dilation
    %se = strel('line',100,0);  % 50 is length of line
```

```
    %gg = imdilate(W,se);
    %se = strel('line',105,0);  % 50 is length of line
    %Wm = imerode(gg,se);
   ss=ss+W;
  %---------------------
  regionstats = regionprops(W, 'all');
  [~, largestidx] = max([regionstats.Area]); %find index of largest region
  %x=regionstats(largestidx).BoundingBox;    %coordinate of bounding box of largest region
  %y=regionstats(largestidx).PixelList;      %coordinate of all pixels in the region as a matrix
   h=regionstats(largestidx).Extrema;        %coordinate of extreme axis
   pcoor = (h(3,:) + h(4,:)).*0.5;
   tip_pos(cuurentframe,:) = pcoor;
   cuurentframe  = cuurentframe + 1;
   %figure; imshow(Q);
% %     figure; imshow(Wm)
%     viscircles(pcoor,10);
%     pause;
%     close;close;
end
disp('Done')
xlswrite( strcat(video_files{vid} , '.xlsx'),tip_pos)
imwrite(double(ss),strcat (video_files{vid}, '.jpg'))
end  % batch loop end
%%
S=double(ss);
imshow(S);
% rectangle('Position',regionstats(largestidx).BoundingBox, 'EdgeColor',
% 'r') %Rectangle to check if flap is detected properly
% imshow(W)
% viscircles(pcoor,10)  TO plot a circle
%%
[temp,originalpos] = sort( h(:,1), 'descend' );
max_num = input('Ist ? max. values to read :');
n = temp(1:max_num); % ist three max values
```

```
p=originalpos(1:max_num); % idx in original array
% [v,idx] = max(h);
val = h(p,2);
fprintf('ist three max values in ist col:\n');disp(n);
fprintf('Corresponding Values in 2nd col:\n');disp(val);
for aa =[1, 2, 3]
   disp(aa)
end
```

MATLAB code for flapping frequency, and amplitude

```
%% filtering matlab
clc
clear all
[v] = xlsread('D6.MP4.xlsx', 'sheet1','D1:D6000');
dt= xlsread('D6.MP4.xlsx', 'sheet1','C1:C6000');
figure(1)
plot(dt,v)
title ('')
xlabel('Time Step')
ylabel('Amplitude')
%% reading of excel file for specified column/values of peak and lower position of flapping
 data = [v];
%A = [ 65 66 67 68 69 70];
%chr = mat2str ([data]);
A = data'
a = max(A);
b = min(A);
c = [a,b];
xlswrite('Delta-Y.xlsx',c);
%% plot magnitude spectrum of a signal
clc
X_mags=abs(fft(v))
figure(2)
```

```
plot(X_mags)
xlabel('DFT Bins')
ylabel('Magnitude')
%% filter
%plot the first half of normalized frequency
%num_bins = length(X_mags);
num_bins = length(X_mags);
figure(3)
plot ([0:1/(num_bins/2 -1):1] , X_mags(1:num_bins/2))
xlabel('Normalizedd frequency ')  %(\pi rads/sample)
ylabel('E')
%% reading of excel file for specified column/values of voltages
 data = X_mags;
%A = [ 65 66 67 68 69 70];
%chr = mat2str ([data]);
B = data'
C =(B(1,5:end))
d = max(C);
e = min(C);
f = [d,e];
xlswrite('Energy Spectra.xlsx',f);
%%
[b_cheby,a_cheby] = cheby1(9, 0.9, 0.02, 'low');
H_cheby = freqz(b_cheby, a_cheby);
%plot filter
norm_freq_axis = [0:1/(512 -1):1];
figure(4)
plot(norm_freq_axis, abs(H_cheby),'r')
legend('Chebyshev')
xlabel('Normalised Frequency');
ylabel('Magnitude')
```

MATLAB code for Amp to Length ratio

```
clc
clear all
close all
I = imread('C0011.MP4.jpg');
imshow(I)
```

MATLAB code for stroboscopic images

```
clc; clear;close all;
%  a =VideoReader('C0536.MP4');
% get(a)
% for img =1:1000:6100
% filename=strcat('frame',num2str(img),'.jpg');
% b=read(a,img);
% c=imcrop(b);
% imwrite(c,filename);
% W=1000;
% end
vidObj = VideoReader('C0005.MP4');
I = read(vidObj,1);
cuurentframe = 1;
[J, rect] = imcrop(I);   % J is image and rect is coor
%vidObj.CurrentTime = 0.0;
Img = 0;
stepSize = 1;
numFrames = ceil(vidObj.FrameRate*vidObj.Duration);
disp('Starting Job')
for Img = 1:stepSize:numFrames
    filename=strcat('frame_',num2str(Img),'.jpg');
    F =  read(vidObj,Img);  % Reads Frame
    Q=imcrop(F, rect); %XY value to crop them in a desired workspace
     fprintf('Current Processing Frame:\t %d\n', cuurentframe)
    Q = rgb2gray(Q);
```

```
    %Q=Q>235;
   % Q = imcomplement(Q);
    imwrite(Q,filename);
end
disp('Done')
```

References

1. Karim, M.E., et al., Energy revolution for our common future: An evaluation of the emerging international renewable energy law. Energies, 2018. **11**(7): p. 1769.
2. Akyildiz, I.F., D. Pompili, and T. Melodia, Underwater acoustic sensor networks: research challenges. Ad hoc networks, 2005. **3**(3): p. 257-279.
3. Ahmed, R., F. Mir, and S. Banerjee, A review on energy harvesting approaches for renewable energies from ambient vibrations and acoustic waves using piezoelectricity. Smart Materials and Structures, 2017. **26**(8): p. 085031.
4. Hou, L. and N.W. Bergmann, Novel industrial wireless sensor networks for machine condition monitoring and fault diagnosis. IEEE transactions on instrumentation and measurement, 2012. **61**(10): p. 2787-2798.
5. Defence, D.o. CONVERTING VIBRATIONS INTO AN ENERGY SOURCE. 2015, ; Available from: https://www.dst.defence.gov.au/innovation/converting-vibrations-energy-source.
6. Kong, H., V. Roussinova, and V. Stoilov, Renewable energy harvesting from water flow. International Journal of Environmental Studies, 2019. **76**(1): p. 84-101.
7. Shi, S., T. New, and Y. Liu, Flapping dynamics of a low aspect-ratio energy-harvesting membrane immersed in a square cylinder wake. Experimental Thermal and Fluid Science, 2013. **46**: p. 151-161.
8. Mehmood, A., et al., Piezoelectric energy harvesting from vortex-induced vibrations of circular cylinder. Journal of Sound and Vibration, 2013. **332**(19): p. 4656-4667.
9. Rupitsch, S.J., Piezoelectricity, in Piezoelectric Sensors and Actuators. 2019, Springer. p. 43-81.
10. Allen, J. and A. Smits, Energy harvesting eel. Journal of fluids and structures, 2001. **15**(3-4): p. 629-640.
11. Goswami, I., R.H. Scanlan, and N.P. Jones, Vortex-induced vibration of circular cylinders. I: experimental data. Journal of Engineering Mechanics, 1993. **119**(11): p. 2270-2287.
12. Latif, U., et al., Experimental investigation of energy harvesting behind a bluff body. Journal of Renewable and Sustainable Energy, 2020. **12**(3): p. 033301.
13. Shan, X., et al., Novel energy harvesting: A macro fiber composite piezoelectric energy harvester in the water vortex. Ceramics International, 2015. **41**: p. S763-S767.

14. Bearman, P.W., Vortex shedding from oscillating bluff bodies. Annual review of fluid mechanics, 1984. **16**(1): p. 195-222.
15. Davidson, J.P., Energy Harvesting for Marine Based Sensors. 2017.
16. Viet, N., et al., Energy harvesting from ocean waves by a floating energy harvester. Energy, 2016. **112**: p. 1219-1226.
17. Yoon, S.J., K. Arakawa, and M. Uchino, Development of an energy harvesting damper using PVDF film. International Journal of Energy Research, 2015. **39**(11): p. 1545-1553.
18. Orrego, S., et al., Harvesting ambient wind energy with an inverted piezoelectric flag. Applied energy, 2017. **194**: p. 212-222.
19. Wang, J., et al., The state-of-the-art review on energy harvesting from flow-induced vibrations. Applied Energy, 2020. **267**: p. 114902.
20. Gao, Y., et al., Effect of surface roughness on vortex-induced vibration response of a circular cylinder. Ships and Offshore Structures, 2018. **13**(1): p. 28-42.
21. Wang, J., et al., Enhancing energy harvesting from flow-induced vibrations of a circular cylinder using a downstream rectangular plate: An experimental study. International Journal of Mechanical Sciences, 2021. **211**: p. 106781.
22. Ding, L., et al., Flow induced motion and energy harvesting of bluff bodies with different cross sections. Energy Conversion and Management, 2015. **91**: p. 416-426.
23. Tamimi, V., et al., Effects of after-body on the FIV of a right-angle triangular cylinder in comparison to circular, square, and diamond cross-sections. Ships and Offshore Structures, 2019. **14**(6): p. 589-599.
24. Vandiver, J. and J.-Y. Jong, The relationship between in-line and cross-flow vortex-induced vibration of cylinders. Journal of Fluids and Structures, 1987. **1**(4): p. 381-399.
25. Sin, V.K., W.Y. Deng, and W.H. Xiao. Study of motion of flexible eel from the wake of bluff body in a cross flow. in AIP Conference Proceedings. 2012. American Institute of Physics.
26. Kazim, M.N.F.M., et al., Analysis of wake region behind bluff body for piezoelectric energy harvester. Journal of Advanced Research in Fluid Mechanics and Thermal Sciences, 2019. **55**(2): p. 249-263.
27. Latif, U., et al., Experimental electro-hydrodynamic investigation of flag-based energy harvesting in the wake of inverted C-shape cylinder. Energy, 2021. **215**: p. 119195.

28. Modir, A. and N. Goudarzi, Experimental investigation of Reynolds number and spring stiffness effects on vortex induced vibrations of a rigid circular cylinder. European Journal of Mechanics-B/Fluids, 2019. **74**: p. 34-40.
29. Zahari, M., et al. The effects of spring stiffness on vortex-induced vibration for energy generation. in IOP Conference Series: Materials Science and Engineering. 2015. IOP Publishing.
30. Saeed, M., et al. Design and development of low-speed water tunnel. in 2018 15th International Bhurban Conference on Applied Sciences and Technology (IBCAST). 2018. IEEE.
31. Content, M. Spring constant. 2022; Available from: https://mechcontent.com/spring-constant/.
32. Roshko, A., Experiments on the flow past a circular cylinder at very high Reynolds number. Journal of fluid mechanics, 1961. **10**(3): p. 345-356.